

A Study of HINS CH Solenoid Axis Determination with Hall Probe Measurements

M. A. Tartaglia, C. Hess

Abstract

Precise determination of the solenoid optical axis is important to achieve the challenging lens alignment tolerances needed to maintain low emittance in the HINS R&D linac transport channel. The translating and vibrating Single Stretched Wire techniques have previously been used to find the solenoid axis [1], and investigations are in progress to understand the sensitivity to construction imperfections in the HINS multi-coil solenoids. An independent approach using a Hall probe to find the axis has been studied by making a series of systematic measurements on a production Type-1 CH solenoid. We describe here the apparatus, data sets, and results of this Hall probe alignment study.

I. Introduction

The tolerances for solenoid positioning in the front end linac transport channel have been under discussion from the start of the HINS R&D effort, and are generally considered to be challenging to achieve at the level of ± 0.15 mm. Recently a numerical study was performed to evaluate the extent to which aberrations from an ideal optical element arise from errors in positioning and due to imperfections in the solenoid lens construction [2]. Imperfections caused by relative displacements of the bucking coils and main coil were of particular concern, as they are not easily distinguished using the Single Stretched Wire (SSW) approaches to finding the axis of the lens. This study concluded that the Main Coil axis, rather than the “average” result obtained from all coils, can in general lead to a closer approximation of the ideal optical axis.

The question of how to assess the Main Coil-only axis position, and more generally how to determine the center line of the individual coils, led to consideration of Hall probe magnetic measurements. Figure 1 shows the dependence of radial field as a function of radius within the aperture, at a sequence of positions along the solenoid length. It is evident that the radial field in the solenoid grows almost linearly with radius around 10 mm from the axis - a convenient position in the lens aperture - at which the radial field strength is reasonably large. Thus, careful measurements of the radial field, made as a function of angle at a fixed radius, should reveal a sinusoidal dependence whose amplitude corresponds to the displacement of rotation axis from the solenoid axis.

Figure 2 shows the radial field versus distance from the solenoid center at a 10 mm radius, separately for the Main Coil (MC), Bucking Coils (BC), and the series combination. The radial field of each coil vanishes at the center of the coil; the radial field shapes are the same, but have opposite sign, at negative Z . This implies that the MC axis can be determined by finding the radial field center at the Z positions of the BCs.

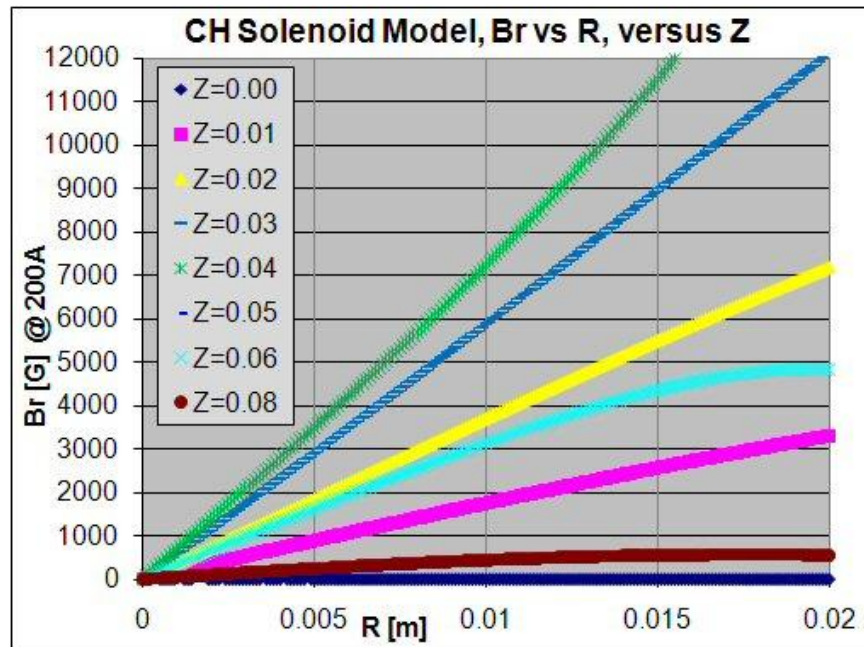


Fig. 1. Radius dependence of radial field versus distance from solenoid center.

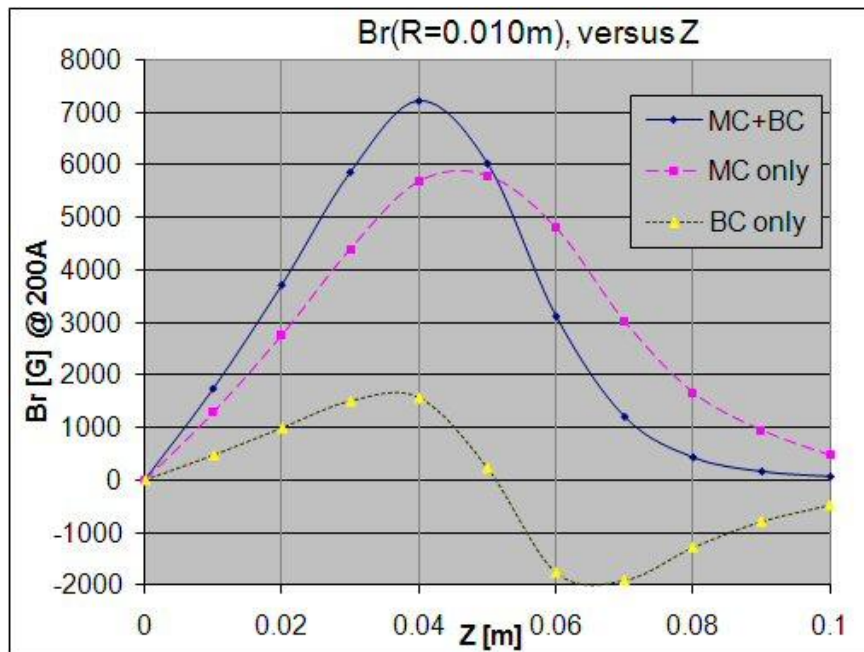


Fig. 2. Radial field versus distance from solenoid center at 1 cm radius.

II. Apparatus

A certification test of the production HINS CH solenoid lens T1_12 (type 1, number 12) was already planned to be made in the MTF stand 3 dewar, and this provided an opportunity to experiment with trying to make precise radial magnetic field measurements. The stand has three pairs of power leads, which allows the choice of powering both individual coils and series

combinations (unlike the production cryostatted lens, in which the coils are internally spliced in series). The stand also has a warm bore tube for CH solenoid magnetic measurements, and a vertical drive system with precision encoder to measure the probe position within 10 microns.

Production magnetic measurements were mostly focused on the axial field strength. To determine the radial field required the assembly of a new probe support and shaft, and the addition of a mechanism for rotating and encoding angular position of the shaft. This apparatus was fairly quickly assembled from parts on hand. One consideration in designing this probe support system was to allow the possibility to also use it in a horizontal orientation, for measuring a production CH cryostat assembly: this constraint limited the radius of the probe support, as the cryostat warm bore has a diameter of only 20 mm.

The probe is shown in Fig. 3 and probe holder in Fig. 4. A Group3 MPT-141-7s transverse Hall probe (S/N 01231225, MTF bar code 0829) is mounted in a G-10 cylinder between the bearings. A machined slot in the cylinder defines the depth of the probe reference surface, which is held flat with two small brass screws that contact it above the slot. This ensures the probe radius is known: measurements (and the probe specification drawing) indicate the probe active element should be at a radius of 7.6 ± 0.1 mm. Figure 5 shows a photograph of the probe holder at the end of a long narrow G-10 shaft. The bearings, made of Delrin® AF plastic, can be replaced if an alternative outer diameter tube (such as the cryostat warm bore) requires.

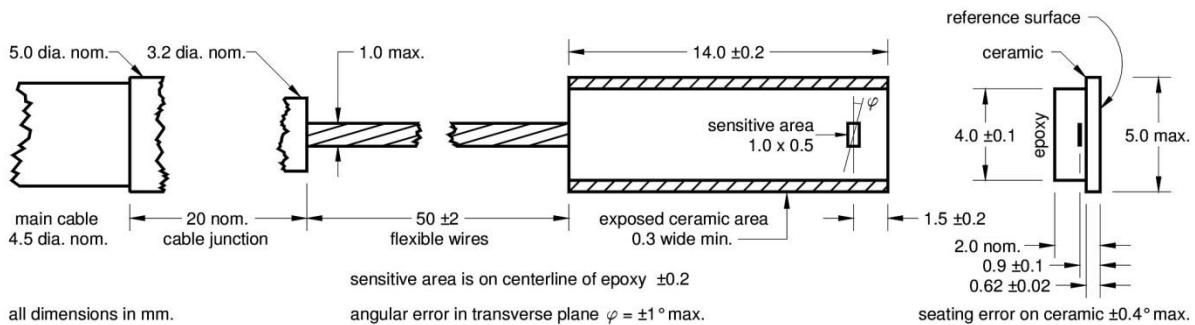


Fig. 3. Group3 MPT-141 Hall probe drawing and dimension specification.

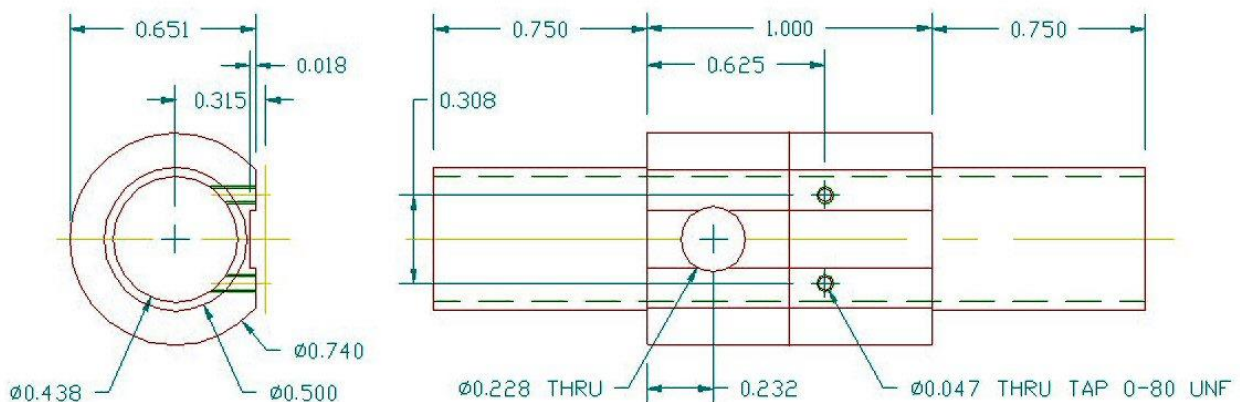


Fig. 4. Drawing and dimensions of G10 probe holder.

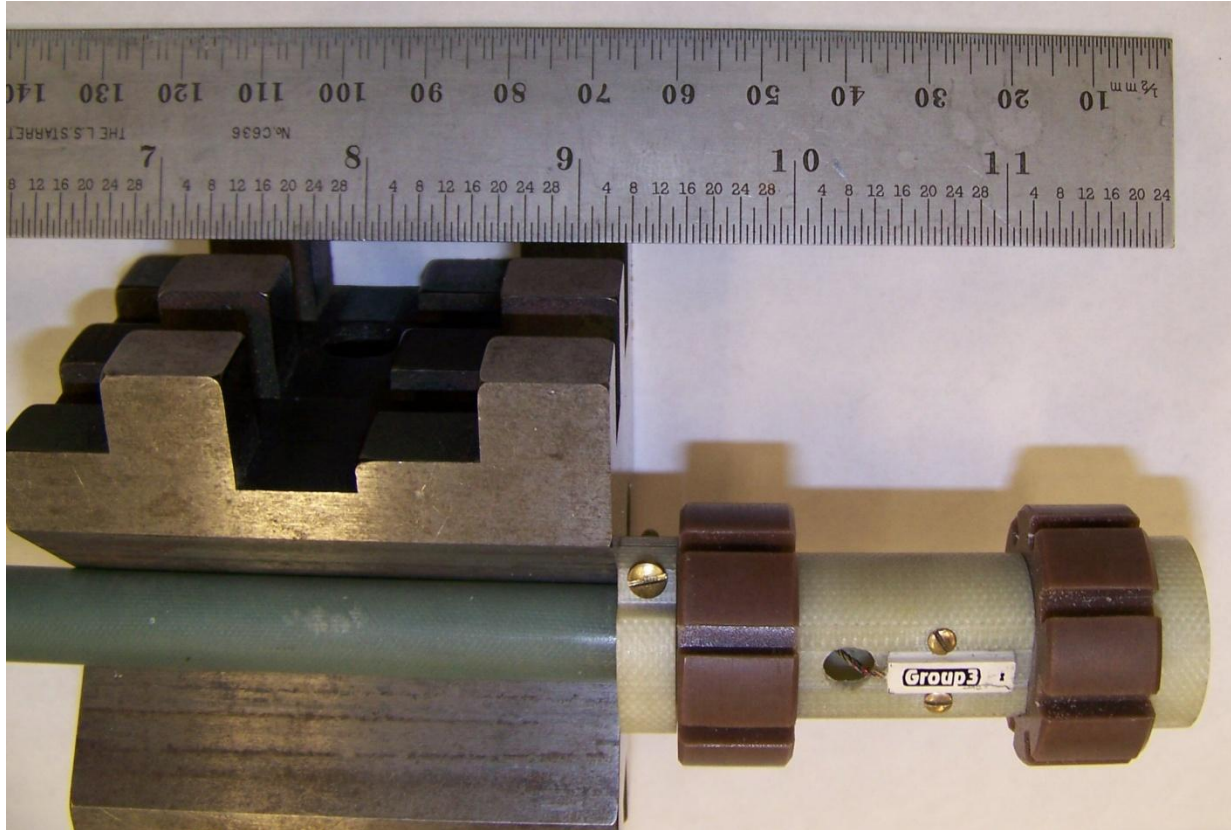


Fig. 5. Hall probe support system for rotation within the stand 3 warm bore tube.

The probe shaft was necessarily quite long. The Hall probe cable was routed through the narrow G10 shaft and brought out at the top, near the coupling to the rotary stage. Also at the top, a gas purge line was connected to force a flow of warm N₂ gas through the shaft into the bore at the probe location, to prevent freezing. The shaft was clamped through a bellows coupling to a rotary stage that was mounted on the stand 3 vertical drive table. Figure 6a shows the wheel (with alignment mark), coupling, probe shaft with emerging cable and gas lines, in situ at the test stand.

The rotary stage was from Newmark Systems, Inc., model RT5DR, S/N 0232. Analog reading of angle positions from the Newmark DRO-1 encoder, S/N 0161, were precise to 2.5 milli-degrees. Figure 6b shows the encoder readout on top, with the dial (green) used for manually rotating the shaft; the small aluminum part below the dial provides an edge by which the zero degree position (facing East) is defined with respect to the alignment mark. This alignment mark is approximately in line with the gas fitting, and the Hall probe radial field direction is about 120 degrees clockwise from this fitting, as seen from the top of the shaft. This information is relevant for later discussion of any offsets in the axis of the solenoid with respect to the rotation axis.

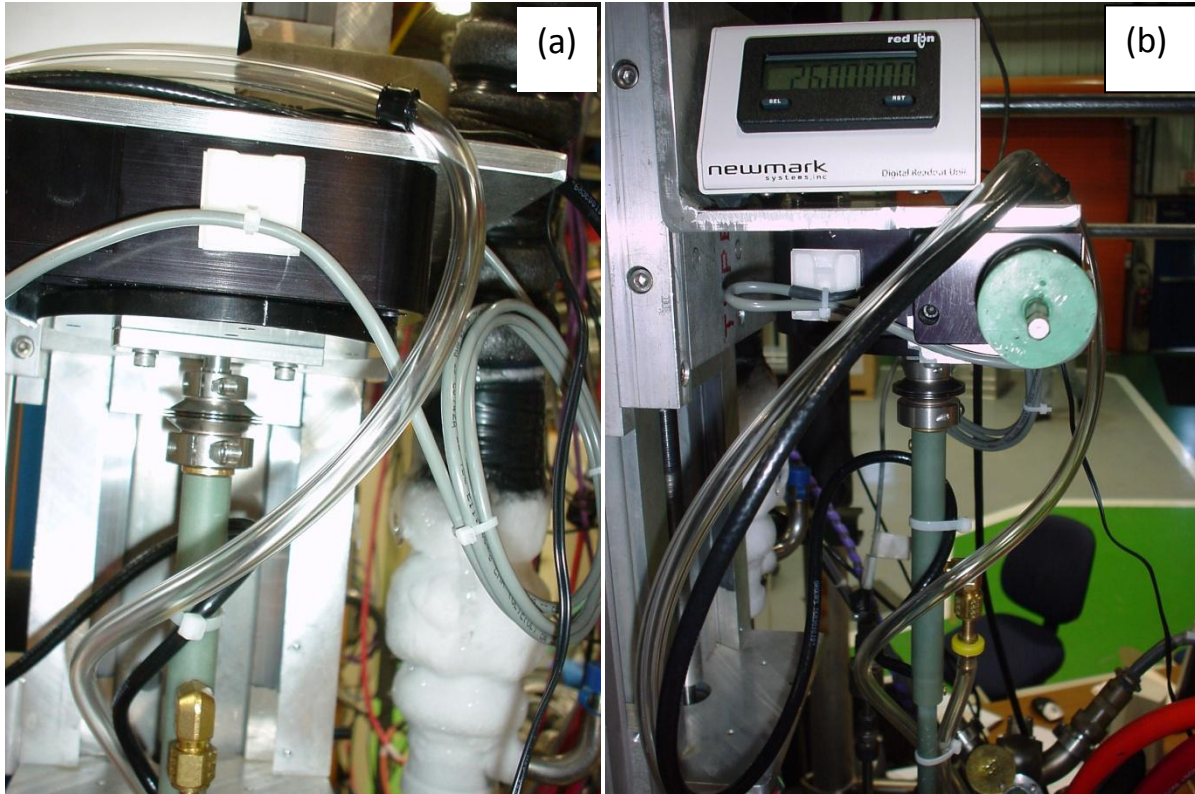


Fig. 6. View showing shaft coupled to rotating ring and orientation of gas fitting with respect to alignment scribe mark (a), and probe angle encoder and motion control knob (b).

III. Data Sets

Since this was a “demonstration” experiment to assess the feasibility, no time was invested in engineering complex motion control or automating data acquisition. Rather, the rotation and vertical positioning was performed manually, and the angle setting (θ) was manually entered into an existing, slightly modified Labview-based Hall probe measurement system. In fact, this was very useful for several reasons: first, it ensured very good control and understanding of the procedure, and allowed some flexibility in repeating or tailoring the measurement plan; second, it allowed the experimenter to observe behavior and respond to problems. In particular, problems with stability in the readings were seen during the initial studies; these were suspected to be caused by flexing of the long shift in response to force applied by the readout cable and gas line, and by vibrations from valves opening, etc. Subsequently, two additional bearings were placed on the shaft approximately 1 and 2 feet above the probe, which appear to have eliminated these sources of error (presumably due to the probe radius changing in response to shaft motion). The probe was not adjusted or removed again until after all measurements were completed, so that angle and Z positions would all be within a consistent coordinate system.

All data were taken with coils powered at 200 A, to obtain reasonably large signals near the solenoid operating point, while remaining comfortably below the quench limit of about 240 A. Three separate data sets were taken, corresponding to the powering of MC+BCs in the standard

series connection arrangement, the MC-only powered, and the two BCs connected in series as they would normally be, but without the MC. These sets should suffice to explore how well one can determine the axis or center position of each individual coil, as well as in the standard arrangement. The solenoid went through a thermal cycle above 200 K in between different power configurations, due to the time (several days) involved in setting up, and this guaranteed that all strand magnetization currents were eliminated at the start of each new set.

For each of these configurations, two independent ways of measuring the field were explored. First, scans of B_r versus Z position were made at fixed angle. These Z scans were made in angle increments of 45.00 degrees (for MC, and BCs) or 90.00 degrees (in the first, MC+BC test), in the range from -180 degrees to +180 degrees. The Z positions of B_r measurements were separated by 10.00 to 10.10 mm (position known to 0.01 mm, but harder to control the actual position to this level), in order to “build up” an angle scan from separate Z scans, yet constrain the expected variation of B_r due to slight variations in Z position. The 10 mm steps were made with respect to the solenoid center, which was initially estimated to be at 273 mm (zero being defined as the probe lowered to the bottom of the warm bore tube); however, it appeared that the actual center may be closer to 275 mm, and some scans were made with that assumption.

Second, at specific Z positions, scans of B_r versus angle were performed in which B_r was measured every 20.00 degrees. In these data sets, the angle was varied over the range -200 to +200 degrees at least, but in many the range was extended from -260 to +260 degrees to study the consistency and reproducibility of points at the same space angle, but taken in different ways. Scans were alternately made either in a Clockwise (CW) rotation of the probe (as see from above, -180 to +180 direction), or in a CCW direction, as it was necessary to unwind the probe cable and gas hose after a full rotation.

At any given (θ , Z) position, a “measurement” consists of a series of Hall probe field values taken for some period of time (of varying length due to manual control of the measurement), generally long enough to determine the scatter and stability of the points. The Group3 Digital Tesla-Meter (DTM-141DG, S/N01340070, MTF bar code 0801) was set to a full range of 1.2 T throughout the test, as some B_r values were seen to exceed 0.6 T (the lowest range, with best resolution) in the preliminary scans. At this setting, the lowest field reading is 0.00002 T, or 0.2 G. The instrument was zeroed (in Earth field) at the start of the test, and checked periodically when the solenoid was warm between configurations; no drift of the zero offset was observed.

IV. Inspection

Following the last set of measurements, while the dewar was still cold, the probe was removed and inspected. First, it was noticed that the Hall probe, support and bearings were somewhat cold (but without frost), and the lower bearing was stiff and not easily turned; the upper bearing moved relatively easily (CTE differs for the G-10 and Delrin® materials). This could explain why, on some measurements, one or more sudden jumps in the Hall probe reading

were observed; such events could be caused by a stick-slip motion in which a bearing hangs up, then releases following a change in the rotation angle. These jumps were generally on the order of 10 G, whereas larger systematic errors in the same scan are at the level of 100 G.

In addition, several measurements were taken of the probe support and bearing dimensions, to establish the actual radius of the Hall element, and the level of mechanical positioning error of the probe. Assuming the Fig. 3 dimensions, the probe radius was 7.6 ± 0.1 mm, as expected. Using a dial gauge, we established that the inner radius of both bearings was about 0.001 to 0.002 inches greater than the G-10 support (when warm); this can introduce about 25 to 50 microns uncertainty in the probe position. This difference could be reduced by using better machine tools than those in the MTF shop, or by adding a thin shim in the existing parts.

However, a much more important source of error was found, in that the bearing outer diameter was substantially less than the warm bore inner diameter. This was quite a surprise to discover; but in retrospect, in order to assemble the apparatus quickly, an assumption about the warm bore inner tube was made, and an existing pair of bearings was chosen that matched the assumed inner bore. The measured bearing outer diameters were 1.174 or 1.175 inches, and the measured warm bore inner diameter is 1.191 to 1.196 inches (possibly not perfectly cylindrical), leaving 0.016 to 0.020 inches, or 0.41 to 0.50 mm difference! The two additional bearings that were added along the shaft are similarly under-sized, so the shaft is not constrained to be on center. **If one assumes that the bearing is always in contact with the inner warm bore tube, this would place the probe at a maximum radius of $7.7+0.05+0.25 = 8.0$ mm around the warm bore tube center.**

After warming up to room temperature, the solenoid assembly was removed from the dewar and careful measurements were made of the warm bore position to determine how well it was centered within the solenoid aperture. Figure 7a shows the top G-10 centering plate with the warm bore in place, as they were lifted from the solenoid; Fig. 7b shows the top of the solenoid, with the bore inserted through the solenoid aperture. A similar plate centers the solenoid on the bottom as well. Welds on the top and bottom of the solenoid helium vessel require that the G-10 groove outer diameter must be slightly oversized, but the warm bore is tightly constrained to be concentric with this outer circle. Thus, it is possible for the warm bore to be slightly offset from the geometric center of the solenoid helium vessel (and, in principle, there can also be slight offsets of the actual solenoid coils from the helium vessel). We measured the gap between the helium vessel inner wall and warm bore outer wall, at four locations – corresponding to East (0.113”), West (0.128”), North (0.106), and South (0.136”) directions during the test (recall that East represents the Zero degree angle). These measurements show an offset of the warm bore with respect to the center of the solenoid aperture, with the center shifted by 0.016”, or 0.41 mm, at an angle 27 degrees West of South; that is, 117 degrees from Zero (CW, as seen from above). Since the Hall probe was approximately 120 degrees from Zero, this would suggest that the greatest amplitude of B_r variations should be along the Zero and 180 degree directions.

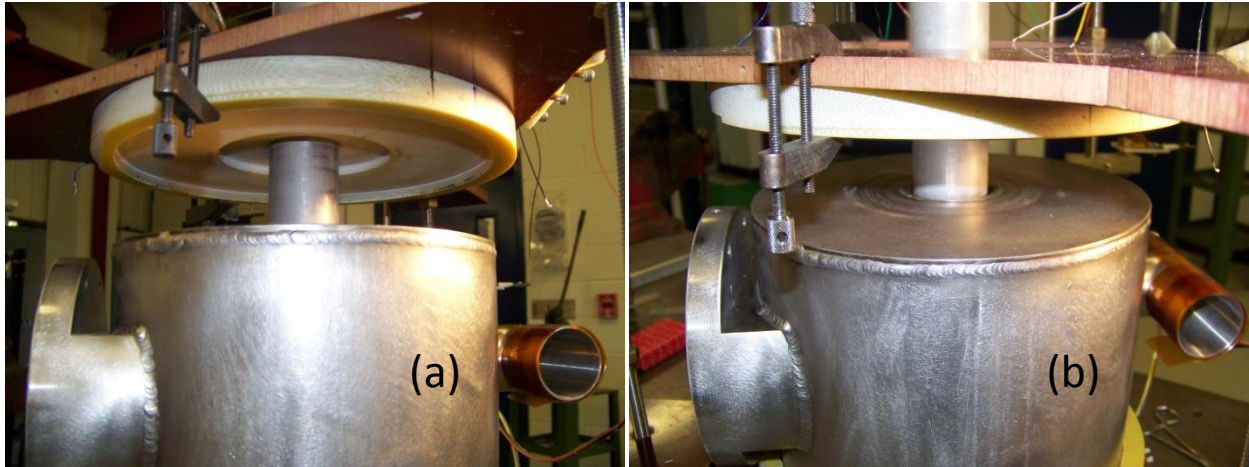


Fig. 7. View of warm bore centered in top support plate (a), and gape between warm bore and solenoid helium vessel aperture (b).

V. Model Predictions

An Opera2D model with geometry corresponding to the vendor-built production magnets was already available and used for defining solenoid performance expectations within the certification process [3]. This model gives absolute predictions for the radial and axial field strength, B_r and B_z , as functions of radial and axial position (R, Z) at the specified current. Previous comparisons to test data [4] show the B_z calculations are valid to 1%. Simulation of the MC-only and BC-only cases was simply made by setting the current density to zero in the unpowered coil(s). Since the model is 2-dimensional, it is azimuthally symmetric by definition. Comparison to data, and determination of axis offsets and tilts, is made by generating tables of B_r and B_z versus Z , at assumed values of R ; then a spreadsheet is used to match model parameters to the observations.

It is interesting to note that the model used originally to compare with data exhibited some not-so-subtle discrepancies in the MC+BC and BC cases, which suggested that something about the geometry was incorrect (profiles did not match well over the entire Z range). Initial thoughts were that shrinkage from cool down might be responsible, but a revised model with 0.3% shrinkage is indistinguishable from the warm geometry. It turned out to be that the pre-production CH solenoid model was being used, rather than the final vendor production as-built design, in which BC geometry is clearly different. Nevertheless, as discussed in the next section, some mismatch in the Z -distributions persists even after the model was corrected.

On closer examination, it was realized that there is some variation in the as-built geometries of the production CH solenoids. The original production as-built model was constructed from the parameters of T1_01, the first solenoid for which numbers were available. Subsequent to the first four magnets, the vendor fabrication travelers changed, and less information was recorded (they no longer contained the coil winding and diameter information, but recorded the coil position information). The model T1_12 tested here differs somewhat from

T1_01 in the MC length and BC locations. Therefore this model was also studied to illustrate systematic variations in the B_r profiles.

VI. Analysis

1) Z-dependence

For each configuration (MC+BC, MC, BC) we made an overlay of the Z scans from data taken at all angles, which are shown in Figures 8, 10, and 12, respectively. There is clearly variation with angle in all data sets, and the extremes in B_r occur consistently at specific angles, θ . Next, in Figures 9, 11, and 13, we plotted only the extreme high and low angle positions from the data and overlaid predictions of the model. In order to make this overlay, the solenoid center position Z_0 is needed; assuming the actual solenoid is symmetric, the best match to the model is for $Z_0=275$ mm. However, there is some asymmetry in the MC and MC+BC cases, in that B_r should vanish at $Z-Z_0 = 0$ but does not (whereas it does for BC case). For MC, this occurs for a center at $Z_0 = 273$ mm, but using this value introduces large discrepancy with the models elsewhere (at the peaks).

Using the minimum and maximum observed variations in B_r , we estimated the range in probe radius needed to match these variations. Most of the data seem to be pretty well circumscribed by the predictions for $R=8.0$ and $R=8.8$ mm, which suggests that the probe is at a radius of 8.4 mm, and the center of rotation is offset from the solenoid center by 0.4 mm. In the BC-only case, a probe radius of 7.6 mm matches the B_r data with minimum excursion (at $\theta = -90$ and -135 deg). Note that the “baseline” model uses the T1_01 geometry, and the T1_12 model has been added to illustrate differences at one radius, 7.6 mm.

Viewed on the full scale of Figures 8-13, the agreement between data and model looks reasonably good. However, a detailed view of B_r in different regions is helpful to see the level of agreement with the model under various assumptions. The detailed views in the region around the solenoid center are shown in Figures 14-16. The “peak” regions are shown in Figures 17 and 18 for MC+BC, Figures 19 and 20 for MC, and Figures 21-24 for BC. Some additional predictions have been added to these graphs to illustrate the effect of a radial tilt of the probe with respect to the solenoid axis. Such a tilt which would add a symmetric (in Z) component of B_z that is not consistent with the data. From Fig. 3, the maximum internal probe tilt error is 0.4 degrees, or 7.0 mrad; other sources of such a tilt could come from the probe mount, or if the solenoid and warm bore tube axes are not parallel. The Figures show B_r+kB_z , where the factor “k” is 0.004, corresponding to a 4 mrad tilt. We observe that there is no evidence of a radial tilt at the level of a few milli-radians (assuming that any such tilt is independent of Z).

Another concern and possible source of error is in the Hall probe output, due to the Planar Hall effect which is proportional to $B_z^2 \sin(2\phi)$, where ϕ is the angle between the field vector and the direction of current flow in the plane of the Hall element [5]. From Fig. 3, the maximum value for ϕ is 1 degree, or 17.5 mrad. Adding such a term to the model prediction does not improve the agreement with the data. The planar Hall coefficient is unknown, but assigning any reasonable value one can see that this term acts similar to a tilt term, being symmetric in Z. It is

conceivable that one could have both tilt and planar Hall terms of opposing sign which might lead to improved agreement with the data: to disentangle the components would require an elaborate effort of multi-parameter, simultaneous fits to the distributions.

From these detail figures, it is clear that there are large discrepancies between the data and model. The level of disagreement is 100 G, which is much greater than the probe resolution. On the other hand, in some regions, the agreement is good. Generally, there is not a close match over the entire range of Z for any of the cases, and furthermore the required large probe radius is not understood (indeed, is believed to be physically not possible). In the ideal situation, we should be able to make absolute prediction of B_r as a function of Z in order to assess the average offset of the axis of probe rotation.

2) Θ -dependence

At a given Z position, we rotate the probe at radius R around the center (X_p, Y_p, Z) with the solenoid axis center at (X_s, Y_s, Z) . Then $\delta R = \sqrt{(X_p - X_s)^2 + (Y_p - Y_s)^2}$. This should result in a sinusoidal variation in the measured B_r , with mean value equal to the predicted $B_r(R, Z)$ and amplitude $B_r(R + \delta R, Z) - B_r(R, Z)$. In general there will be a phase shift ϕ needed to align our arbitrary measurement coordinate system (defined by $\theta = 0, 90$) with the vector $(X_p - X_s, Y_p - Y_s)$.

First, comparison of angle scans at fixed z, with z-scans at fixed angle are made. Table 1 summarizes the parameters for the angle scan data sets that were captured, and the corresponding closest Z position at which data exist for comparison with Z scans, taking $Z_0 = 175$ mm. These overlays show again that the absolute prediction for average B_r requires some adjustment of the Z position, by up to ± 2 mm in some cases. Nevertheless, they agree pretty well, assuming the larger-than-expected probe radius.

Table 1. Closest positions (Z-Z₀) of measured B_r versus θ in Angle and Z scans.

MC+BC, Z-175 [mm]		MC-only, Z-175 [mm]		BC-only, Z-175 [mm]	
Angle Scan	Z Scan	Angle Scan	Z scan	Angle Scan	Z scan
-55.4	-50, -60	-52	-50	-62	-62
-42	-40	-42	-40	-32	-32
+38	+40	+38	+40	+38	+38
+51.5	+50, +60	+48 CW, CCW	+50	+68	+68

Second, we overlay the data with sinusoidal functions based upon model expectations (i.e., assuming the probe radius of 8.4 mm, and $\delta R = 0.4$ mm, from the earlier Z-dependence study); all measurements (from $\{-260, 260$ deg $\}$) are folded into the angle range $\{-180, 180$ deg $\}$, which allows comparison of the measurement consistency. These show fairly good agreement in angle distributions. Note that there appears to be a systematic tendency for points in certain angle ranges to be non-sinusoidal and have wider variation – particularly around ± 135 degrees. These distributions are shown in Figures 25-26 (MC+BC), 27-29 (MC) and 30-31 (BC).

So far, the angle analysis has been qualitative and semi-quantitative. To be more rigorous, we used MATLAB to fit each of the data sets to a three parameter sinusoidal function, $B_r(\theta, Z) = \langle B_r(Z) \rangle + A(Z) \cdot \sin(\theta + \varphi)$, where $\langle B_r(Z) \rangle$ is the average radial field strength at the position Z , A is the amplitude of the sinusoidal variation with angle θ , and φ is the phase angle. Thus the fit forces the sinusoid to be a single period within the $\{-180^\circ, 180^\circ\}$ angle range. The MATLAB fitting function finds a least squares solution starting from a random seed for the 3 function parameters, and may settle into “local” minima that are not always reasonable solutions. Thus, visual inspection of the fits was necessary to select the best results; on the whole, they are quite good, with the phase angle being the most uncertain – at the level of about 5-10 degrees. Animated GIF files illustrating the fits to all of the angle data are accessible from the following links:

http://tdserver1.fnal.gov/tartaglia/documents/Projects/HINS/ProductionTesting/MCBC_Fits_AnimationByZ.gif

http://tdserver1.fnal.gov/tartaglia/documents/Projects/HINS/ProductionTesting/MC-only_Fits_AnimationByZ.gif

http://tdserver1.fnal.gov/tartaglia/documents/Projects/HINS/ProductionTesting/BC-only_Fits_AnimationByZ.gif

The results of these fits are plotted in Figures 32-34, respectively comparing the distributions of $\langle Br \rangle$ vs. Z , Amplitude vs. Z , and Phase angle vs. Z for the data sets (a) MC+BC, (b) MC-only, and (c) BC-only. Model overlays are made for (a) and (b), assuming a probe radius of 8.4 mm. First, it is clear that the data and model agree well for (a), but not (b); also, there is very good agreement of the fit parameters for the Angle and Z -scans Scans, which gives confidence that the Z scan results can be taken seriously over the entire Z range (even in the MC+BC case, for which the data were taken only in 45-degree steps!).

Second, there are some striking features evident in these figures. An apparent shift or “discontinuity” in the fit amplitude near the solenoid center seems to be real – it exists in both the MC and MC+BC data, but not the BC data. This is not so much a discontinuity, as an indication that the variation with angle is larger than expected in some regions: Figure 35 shows this by plotting the absolute value of the MC amplitude versus Z position, showing that it does not go to zero at the center, but maintains some positive value. The amplitude variations for the individual coils exceeds the expected value in the region of the peak, but is pretty good in the tails; on average, these excursions cancel for the MC+BC to give about the right values. Finally, the phase angles show variation with position that is somewhat different for the MC and BC – which could be an indication of what we are interested to know: is there a relative shift of the BC’s from the MC axis. On the other hand, the MC phase changes with position: one thought is that perhaps this is due to an asymmetry in the coil about the Z axis. An eccentricity in the azimuthal shape, which could vary with Z , might explain both the phase angle changes and the greater-than-expected excursions in radial field amplitude. A 3D model could be used to study how large such an effect might be. It will certainly be interesting to gather data on additional solenoids (this is planned, at least for the first production CH cryostat assembly). A BC phase angle shift could result if the BCs are tilted with respect to the warm bore tube axis.

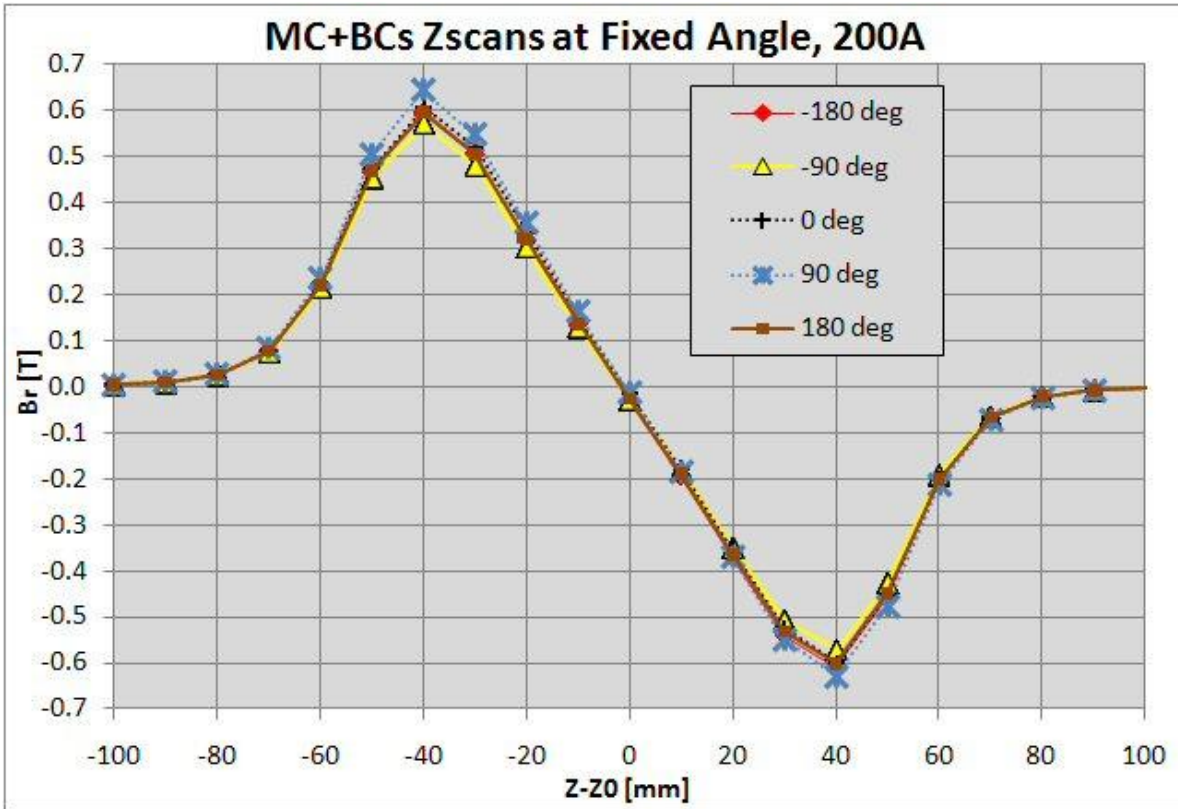


Fig. 8. Profiles of radial field versus Z position at all angles for MC+BC powered at 200 A.

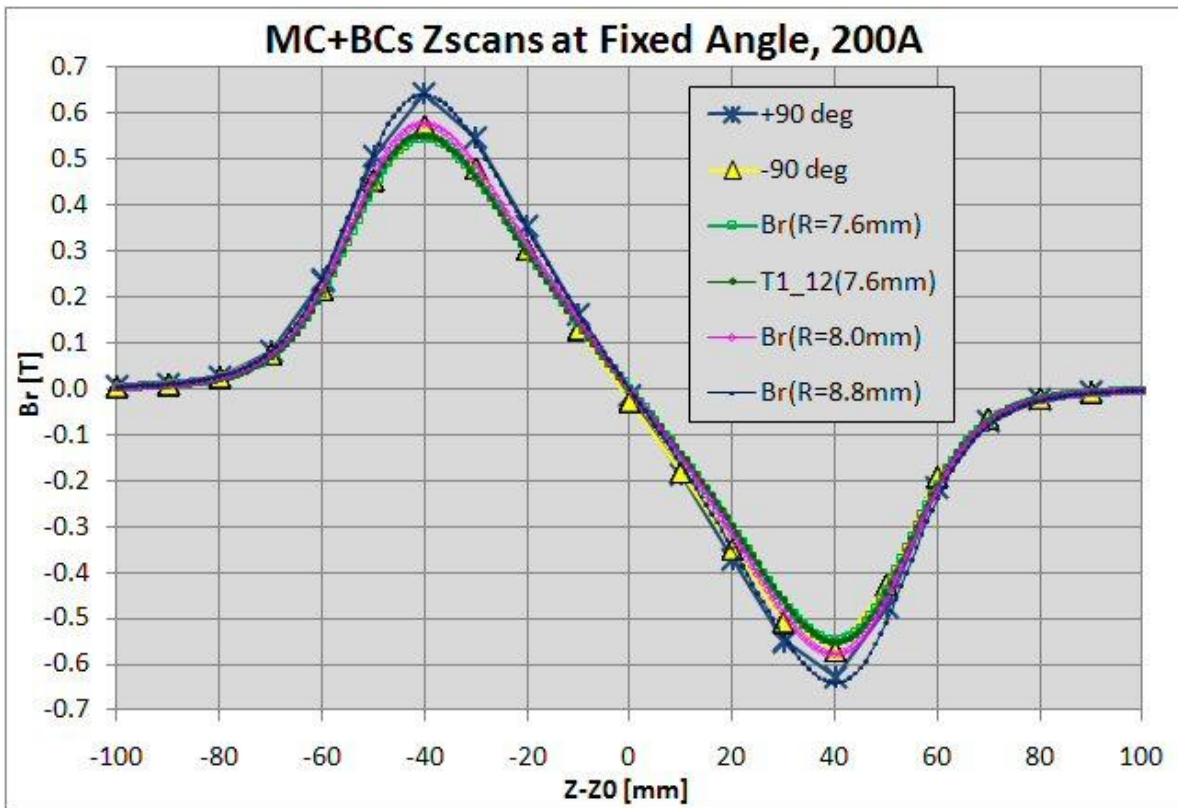


Fig. 9. Data (extremes) and model comparison of radial field Z-profiles for MC+BC.

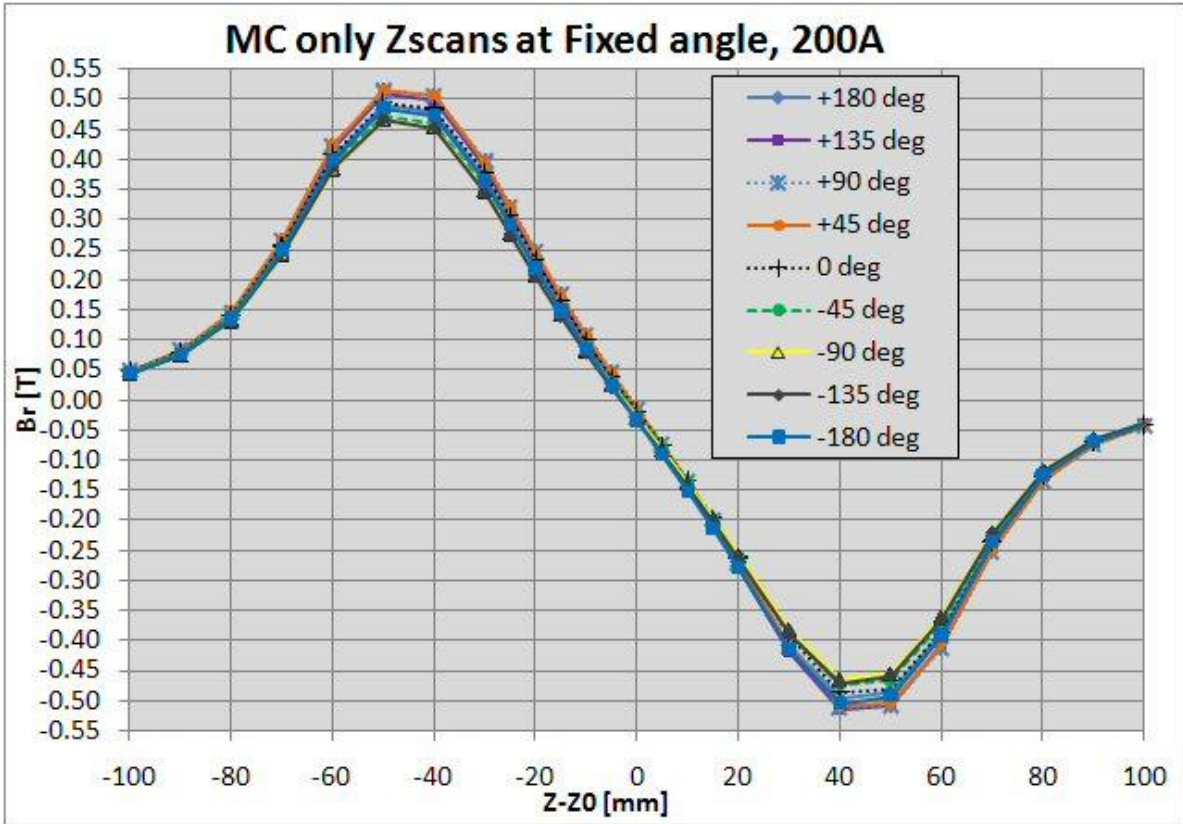


Fig. 10. Profiles of radial field versus Z position at all angles for MC powered at 200 A.

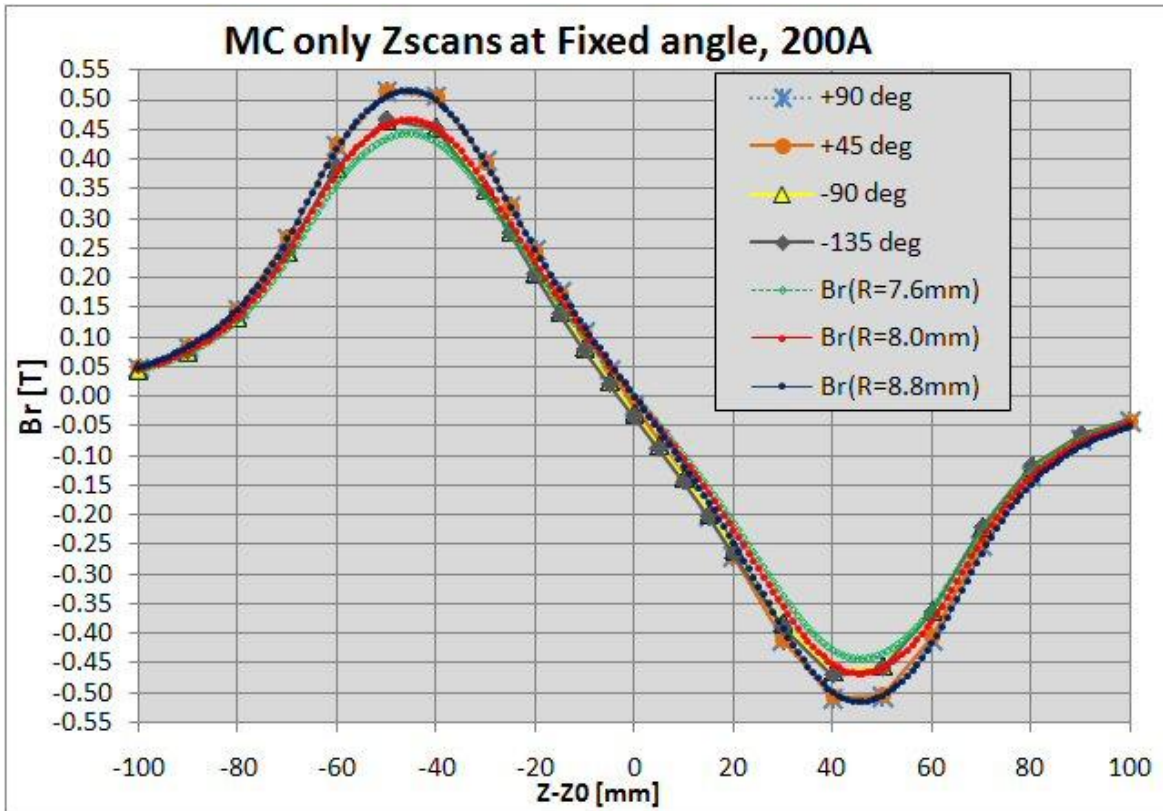


Fig. 11. Data (extremes) and model comparison of radial field Z-profiles for MC.

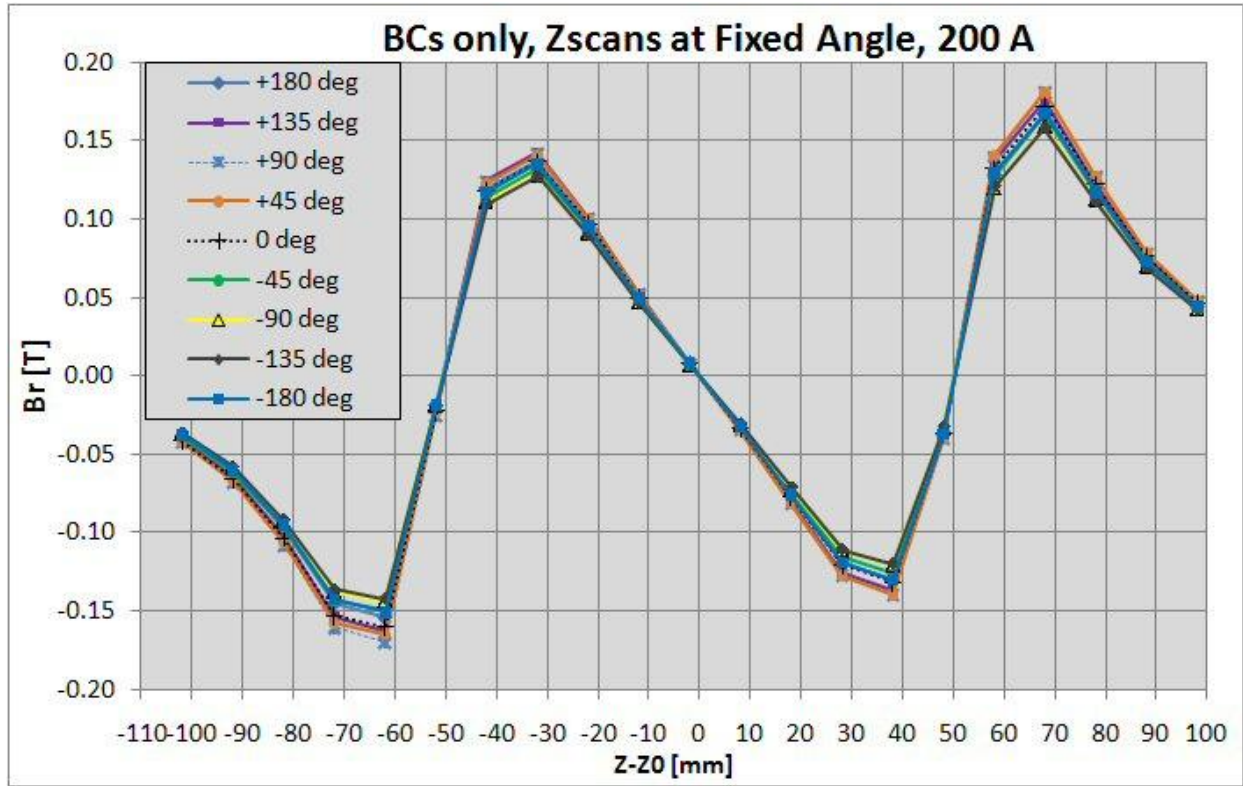


Fig. 12. Profiles of radial field versus Z position at all angles for BC powered at 200 A.

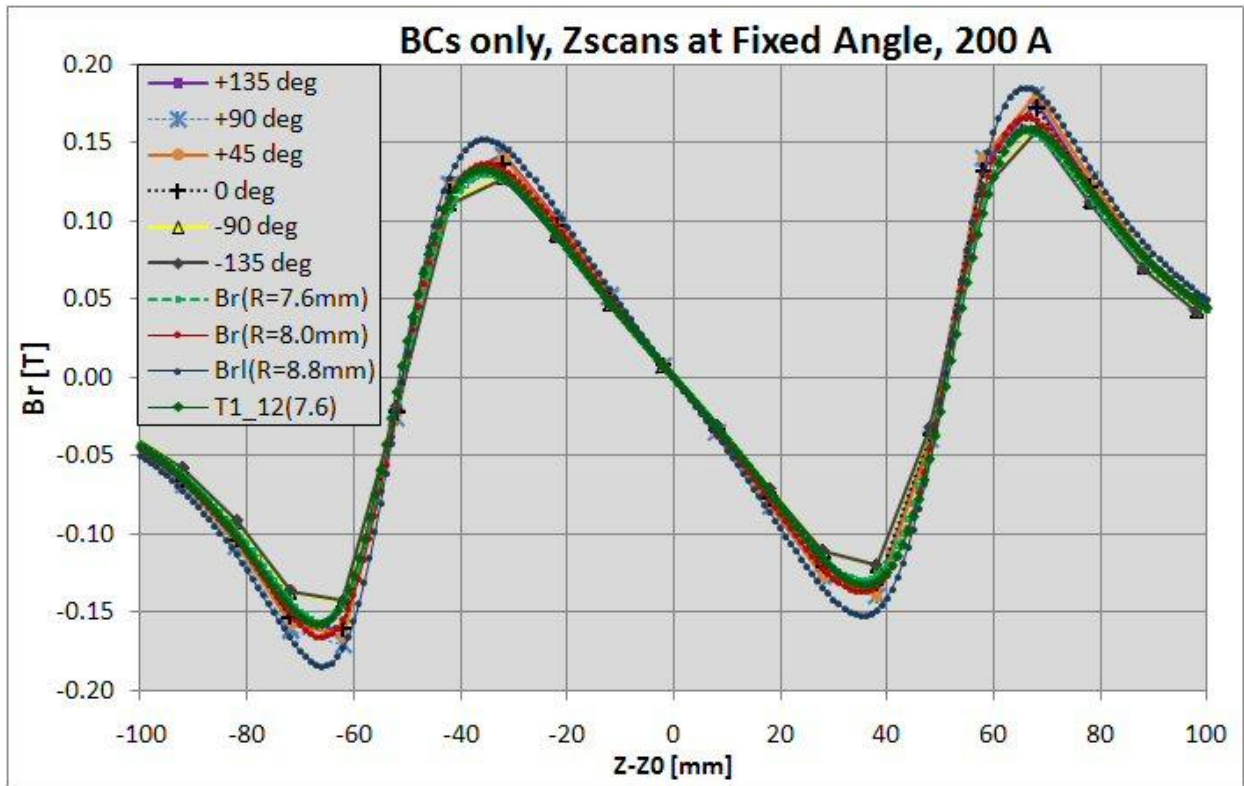


Fig. 13. Data (extremes) and model comparison of radial field Z-profiles for BC.

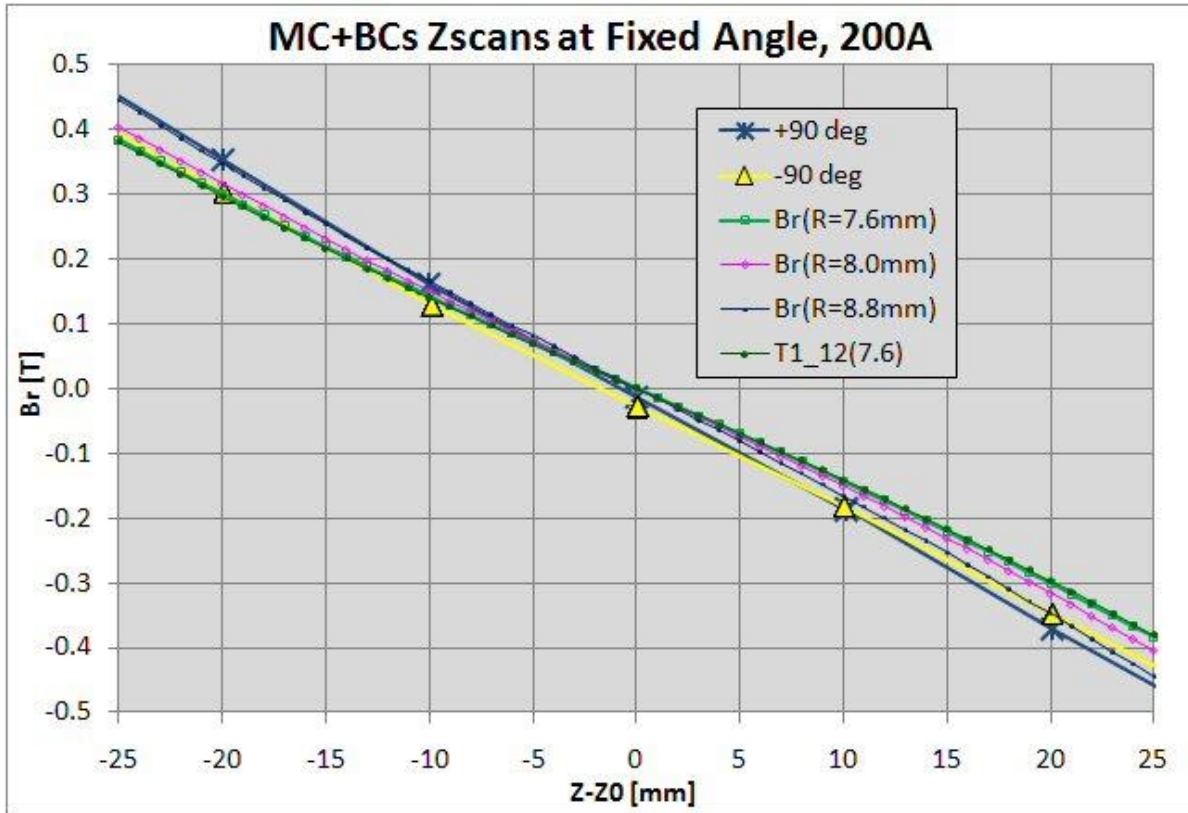


Fig. 14. Detailed B_r data and model comparison for MC+BC near the solenoid center.

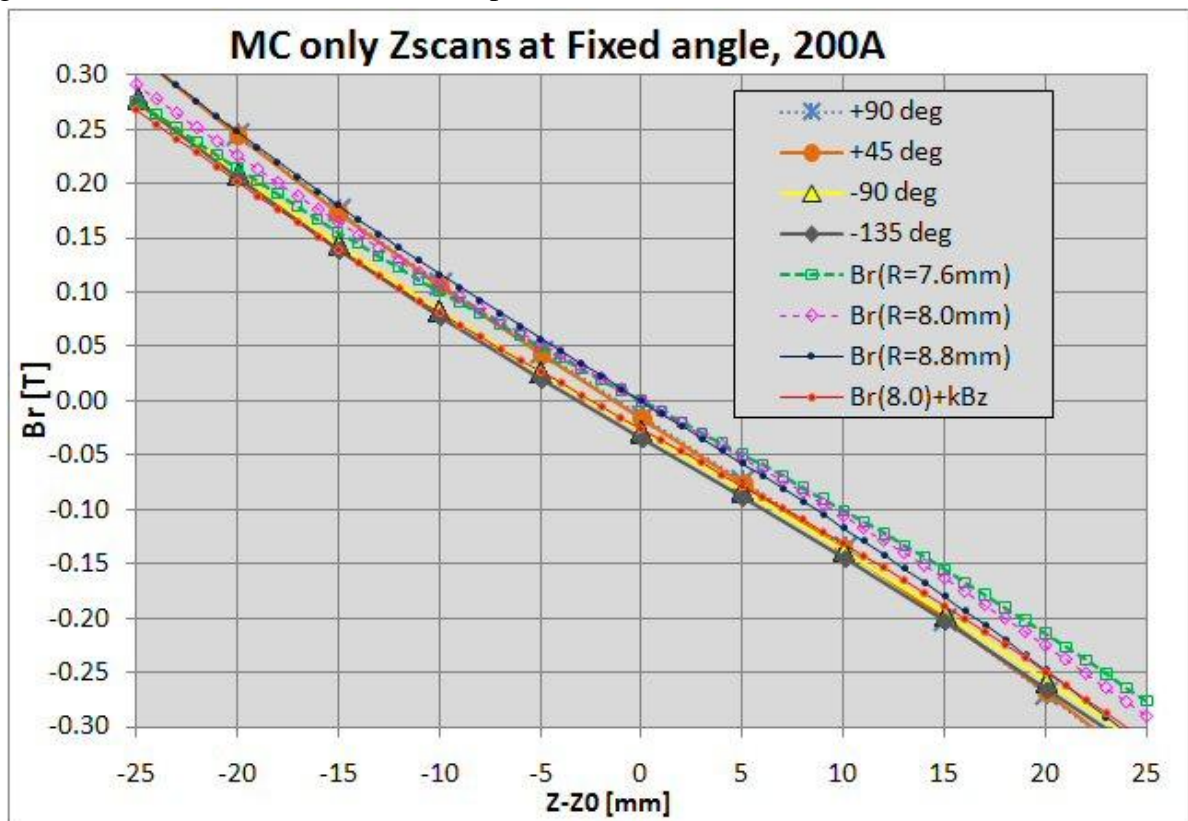


Fig. 15. Detailed B_r data and model comparison for MC near the solenoid center.

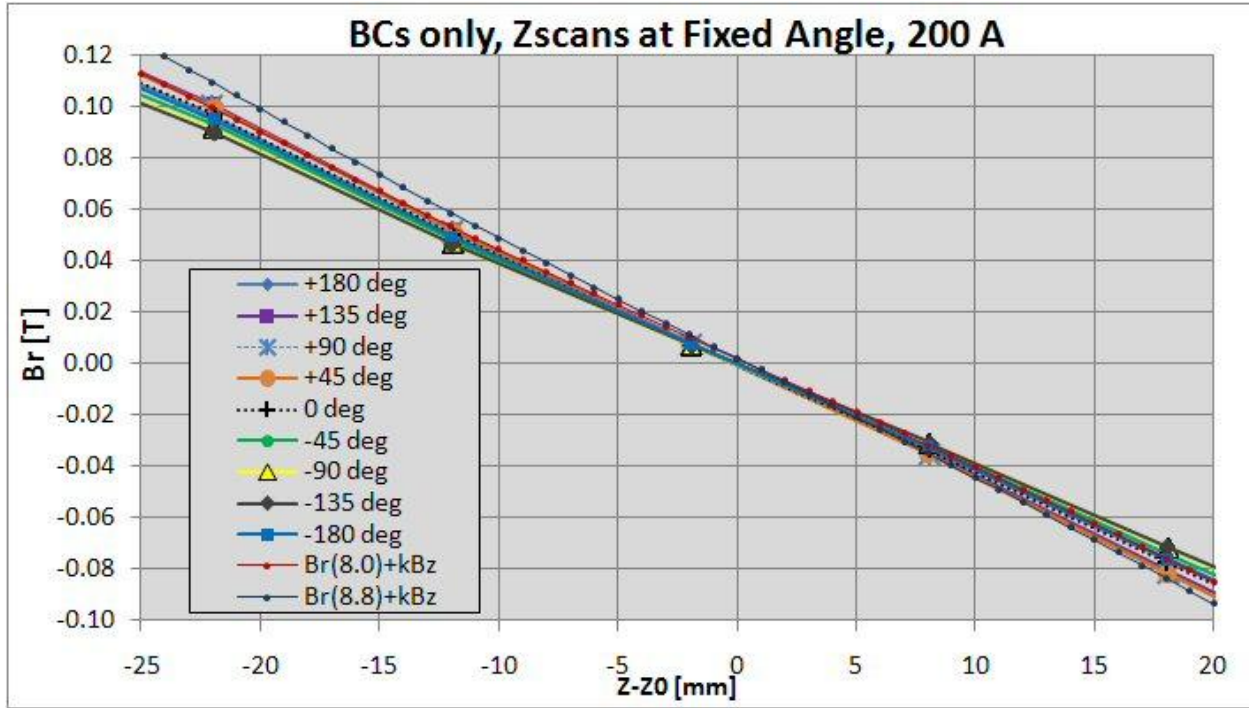


Fig. 16. Detailed B_r data and model comparison for BC near the solenoid center.

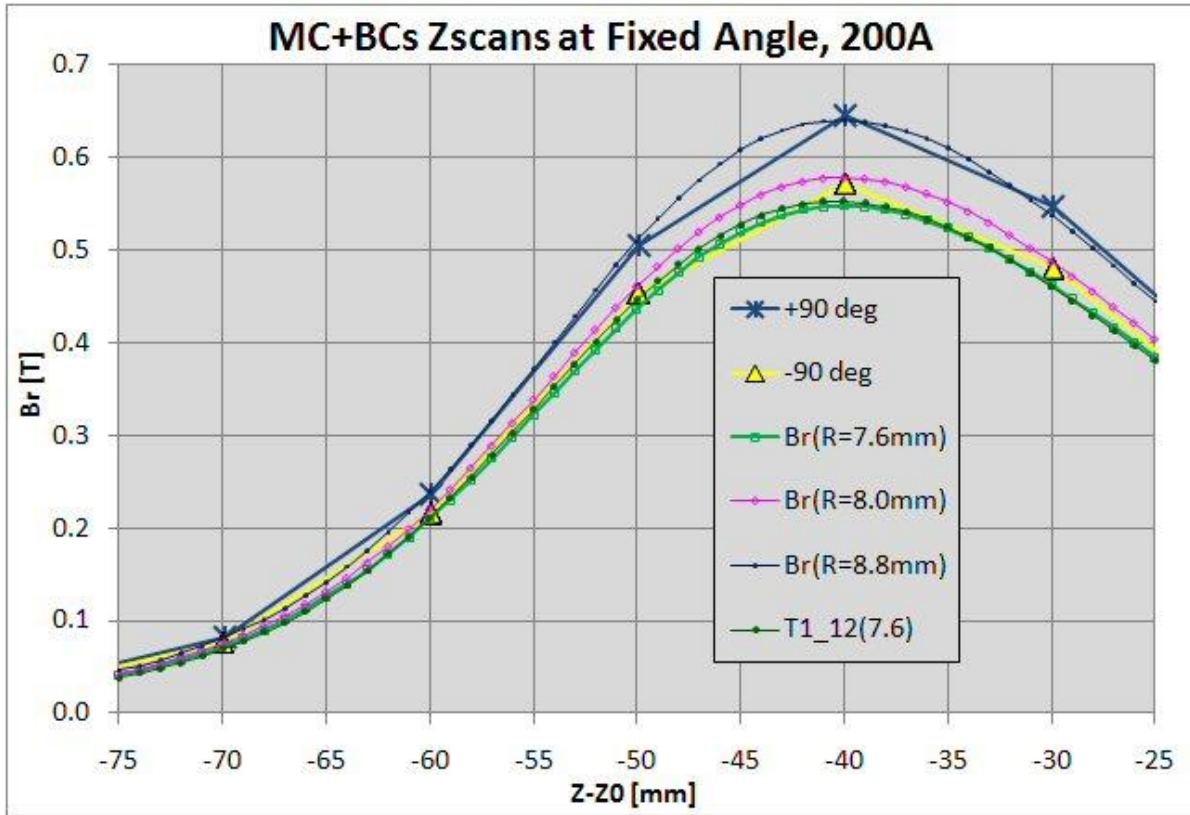


Fig. 17. Detailed B_r data and model comparison for MC+BC at negative $Z-Z_0$.

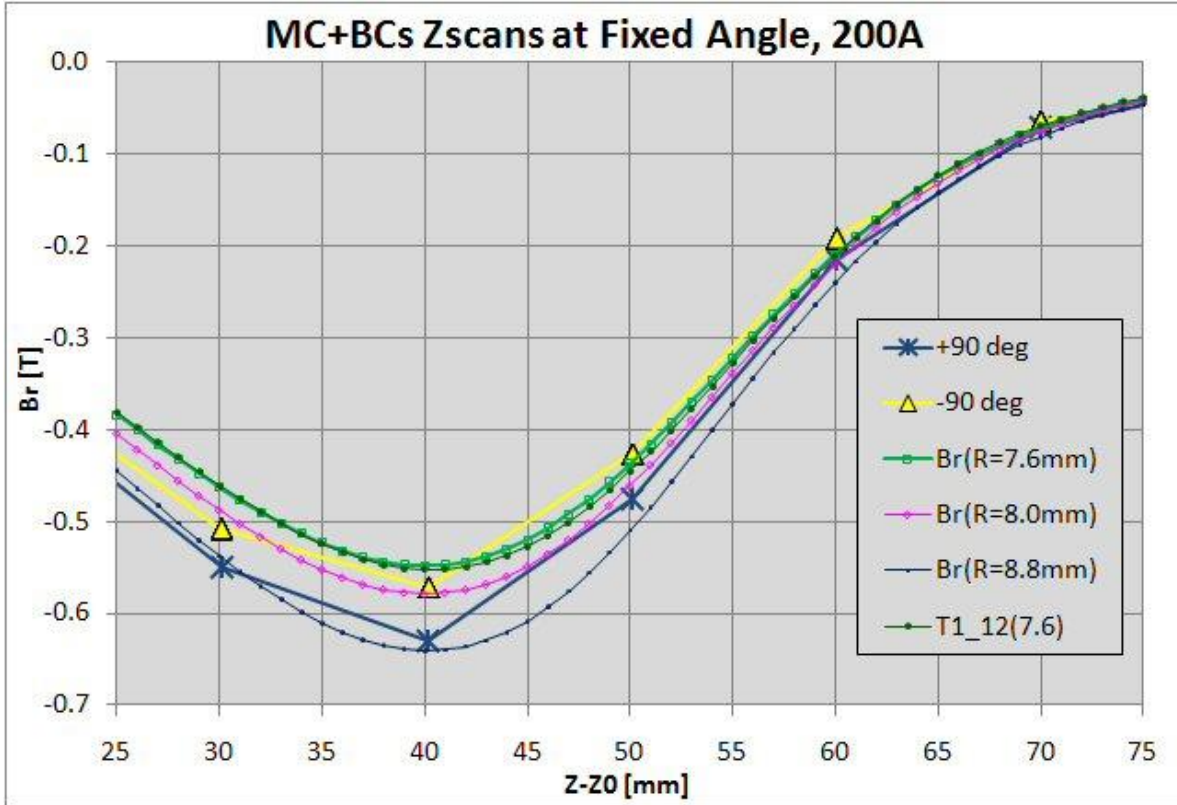


Fig. 18. Detailed B_r data and model comparison for MC+BC at positive $Z-Z_0$.

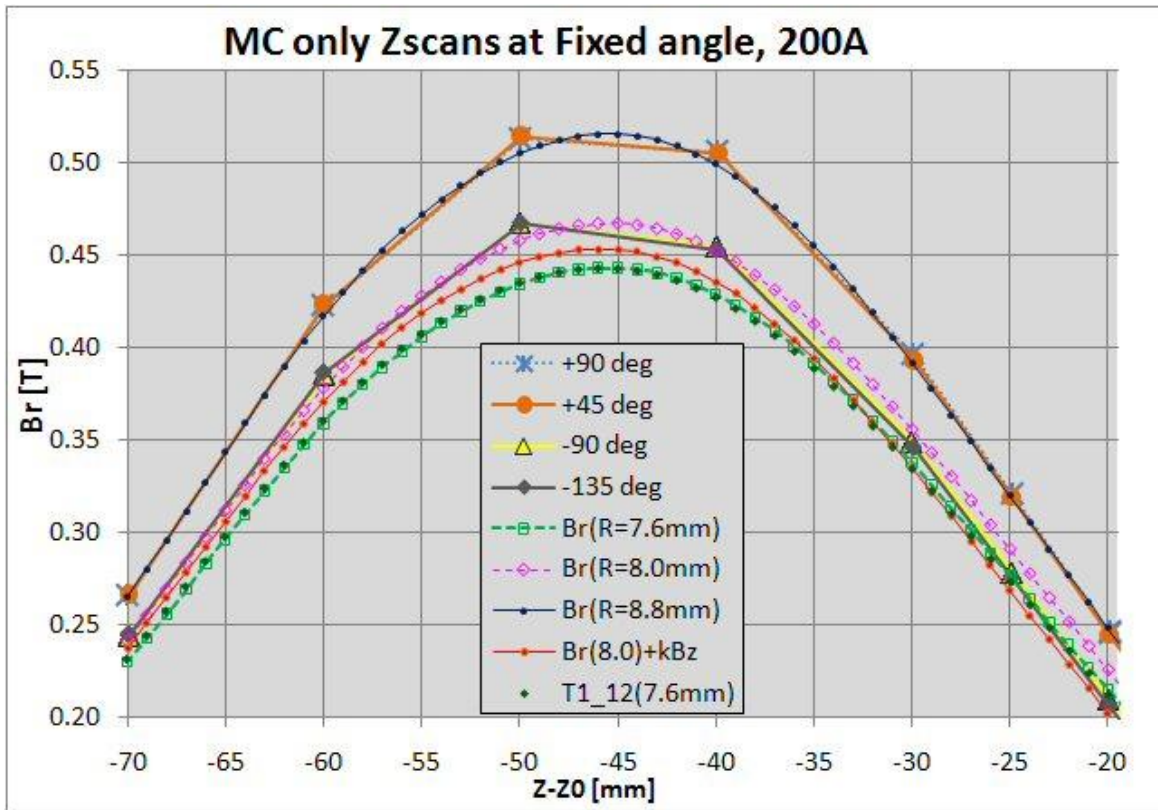


Fig. 19. Detailed B_r data and model comparison for MC at negative $Z-Z_0$.

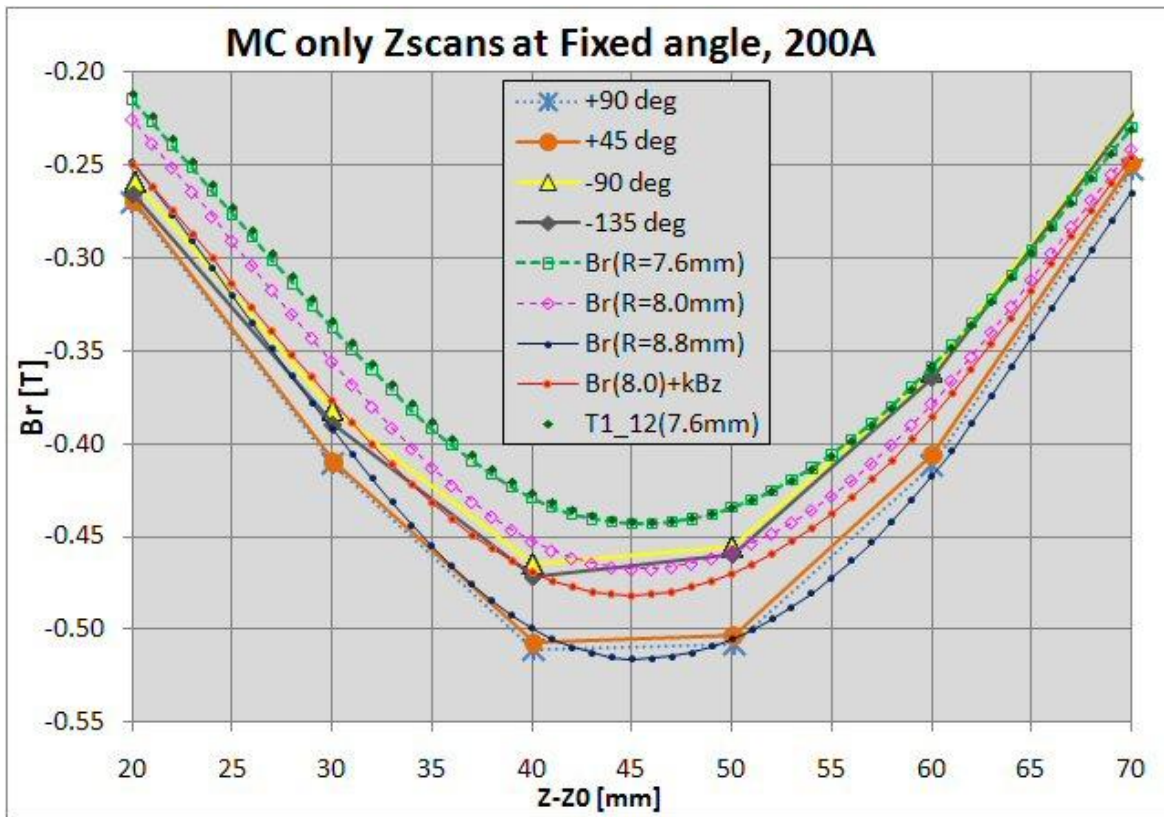


Fig. 20. Detailed B_r data and model comparison for MC at positive $Z-Z_0$.

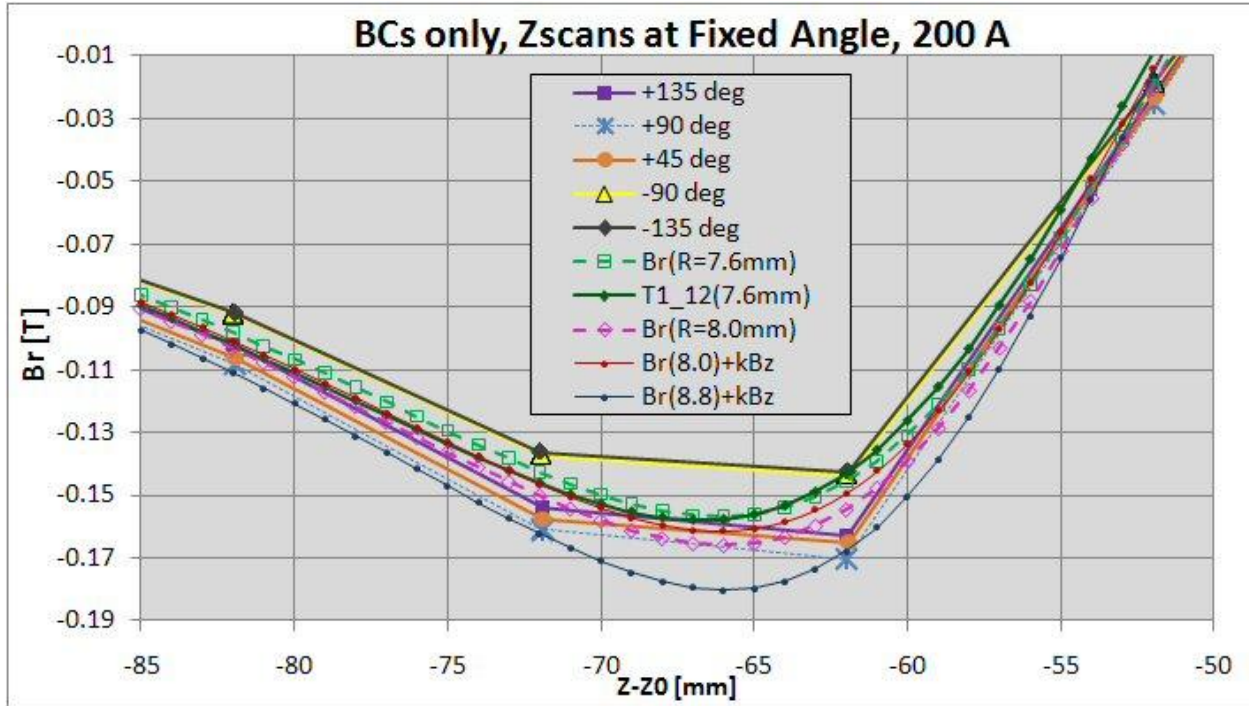


Fig. 21. Detailed B_r data and model comparison for MC at far negative $Z-Z_0$.

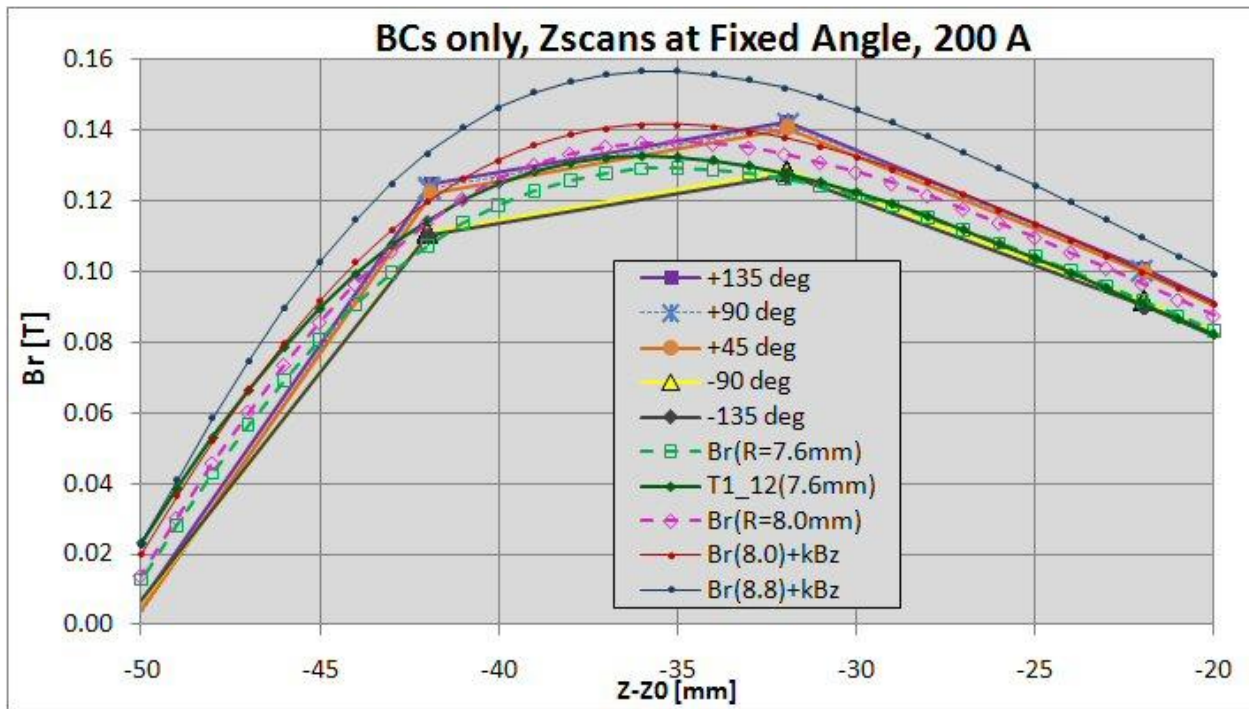


Fig. 22. Detailed B_r data and model comparison for MC at near negative $Z-Z_0$.

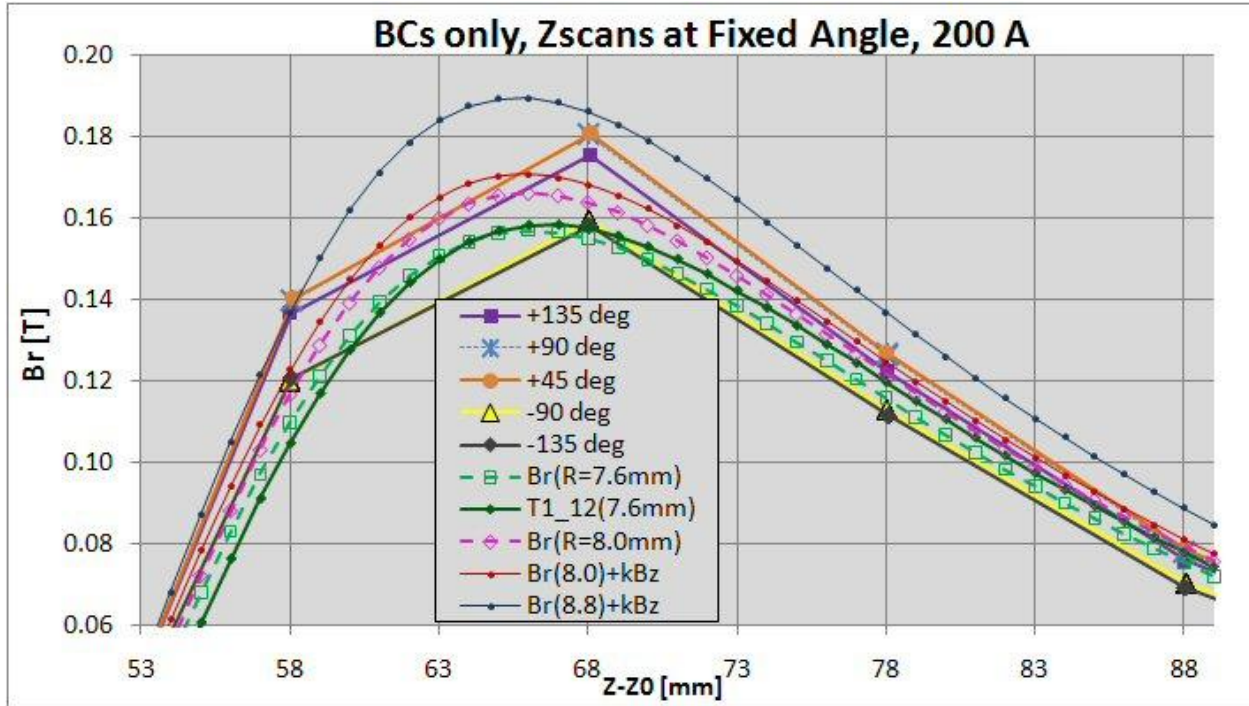


Fig. 23. Detailed B_r data and model comparison for MC at far positive $Z-Z_0$.

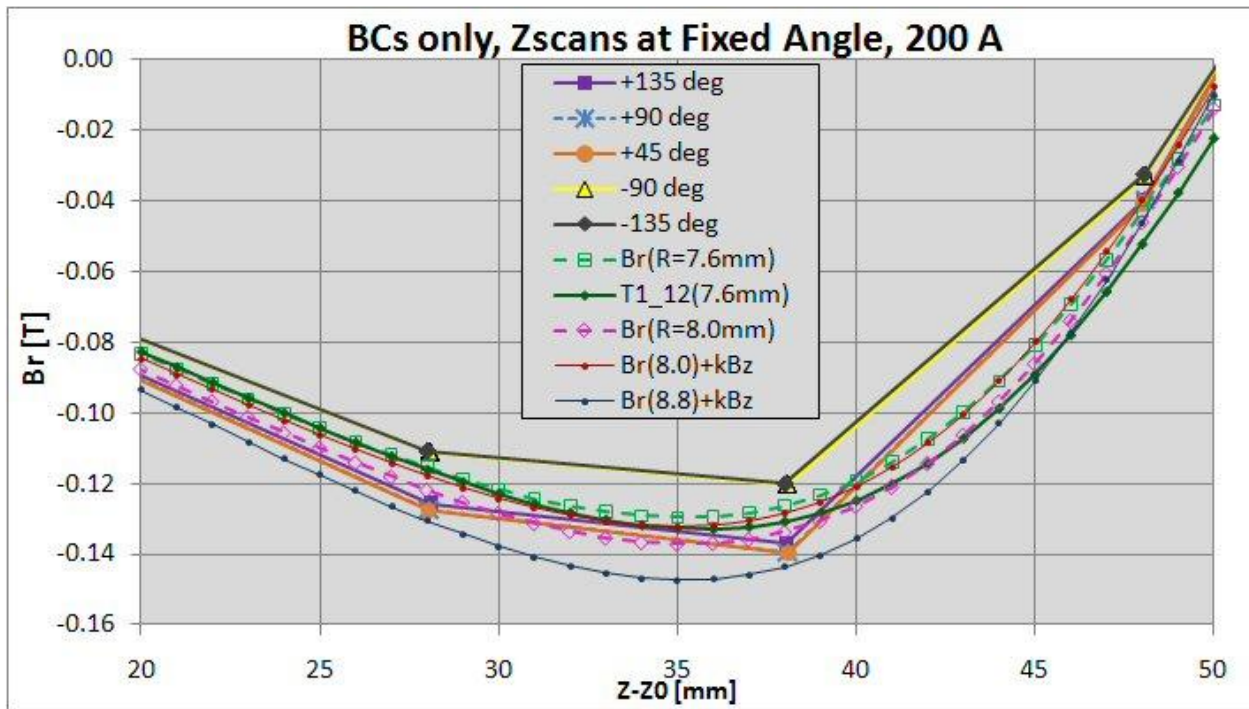


Fig. 24. Detailed B_r data and model comparison for MC at near positive $Z-Z_0$.

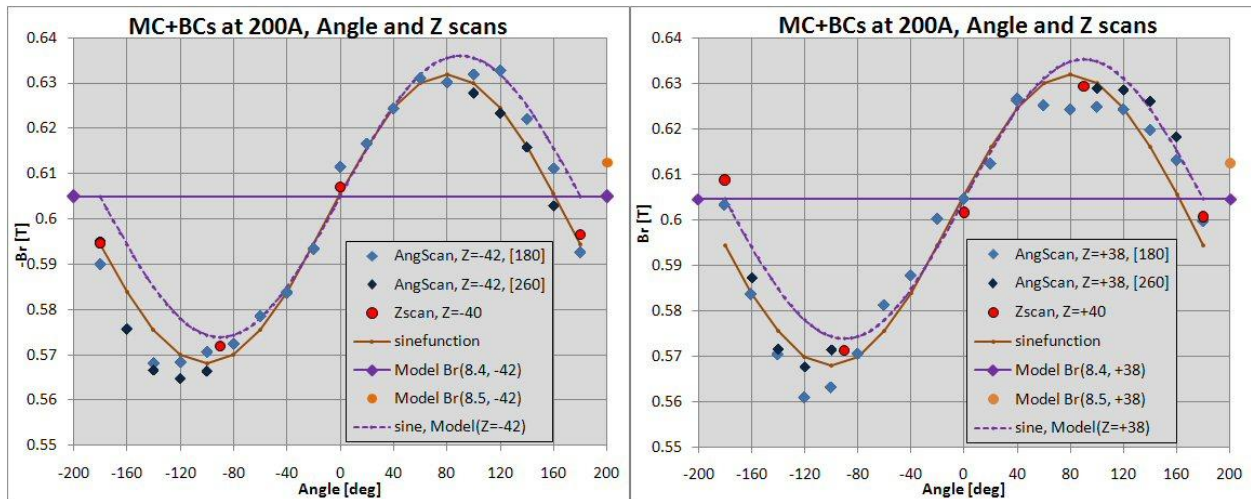


Fig. 25. Angle dependence of data for MC+BC Angle scans at $Z=175=-42$ mm ($-B_r$ left) and $Z=175=+38$ mm (B_r right), and Z scans at $|Z-175|=40$ mm. Average B_r are shown for the as-built model at the appropriate Z positions. Two sinusoidal functions are shown: one uses the model parameters (dashed violet lines) and has an offset angle of zero; the other (solid brown lines) use an “eyeball fit” for the mean and amplitude, with a 10 degree offset angle.

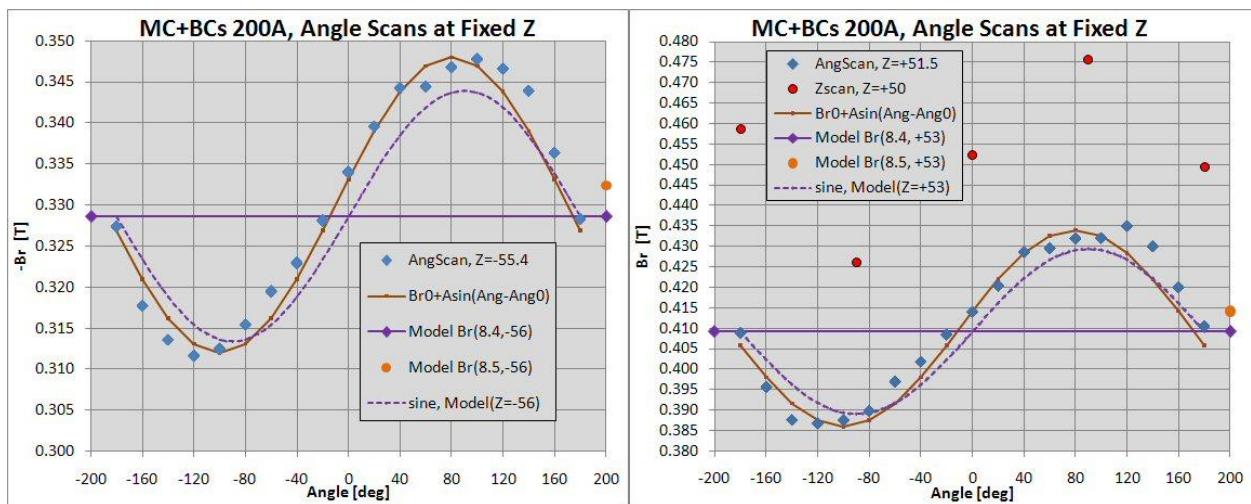


Fig. 26. Angle dependence of data for MC+BC Angle scans at $Z=175=-55.4$ mm ($-B_r$ left) and $Z=175=+51.5$ mm (B_r right); Z scans are not shown on left figure (closest Z positions were 50 and 60 mm, so direct comparison is not very informative). Model and “eyeball fit” sine functions are plotted with the same parameters indicated in Fig. 25.

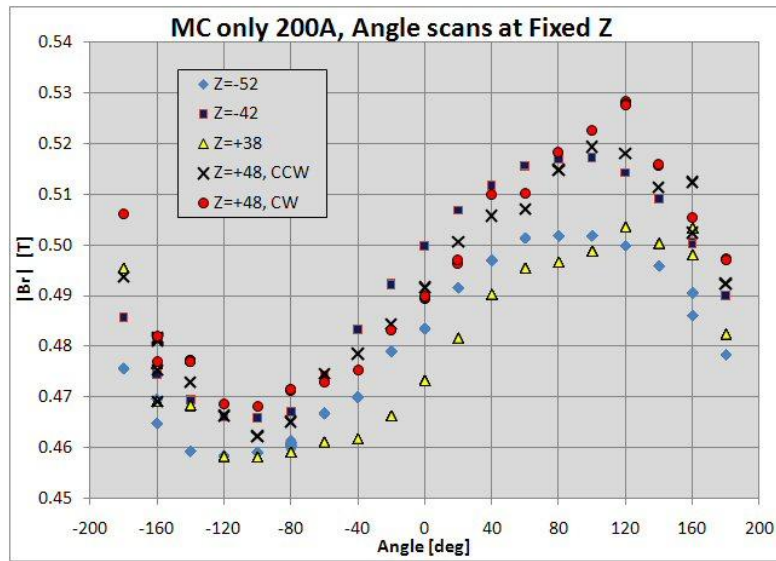


Fig. 27. $|B_r|$ data for all MC Angle scans are superimposed, to show the level of variation in the angle dependence. This is possible because the values do not change much for the MC-only case in this Z region, where B_r is peaked (e.g., see Figs. 19 and 20).

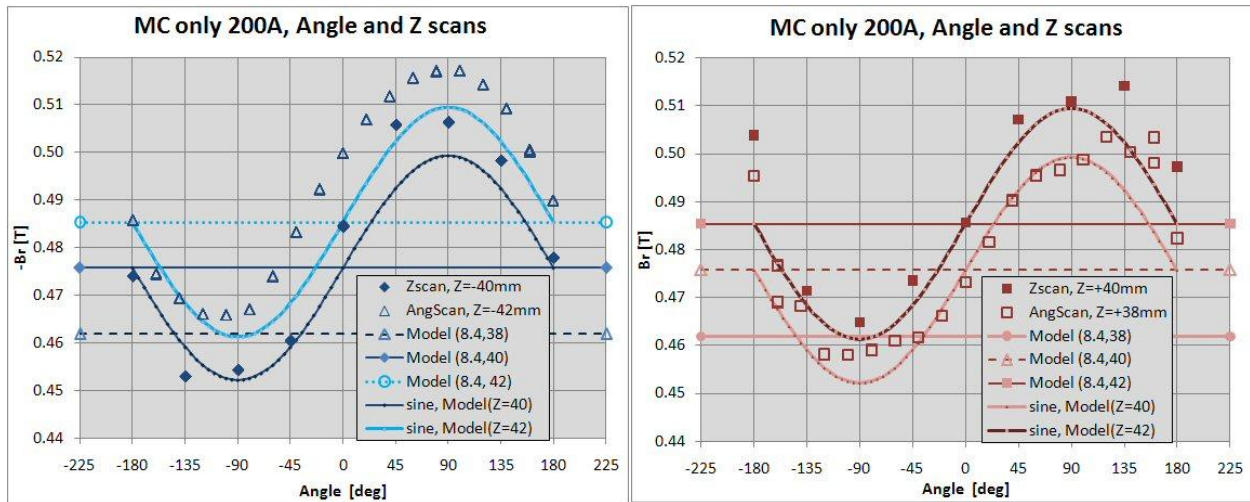


Fig. 28. Angle dependence of B_r data for MC Angle Scans at $Z=175=-42$ mm ($-B_r$ left) and $Z=175=+38$ mm (B_r right), and Z scan data at ± 40 mm. Average B_r are shown for the as-built model at the same and nearby Z positions. Sinusoidal functions using the model parameters (and no angle offset) are plotted for some of the Z positions for comparison.

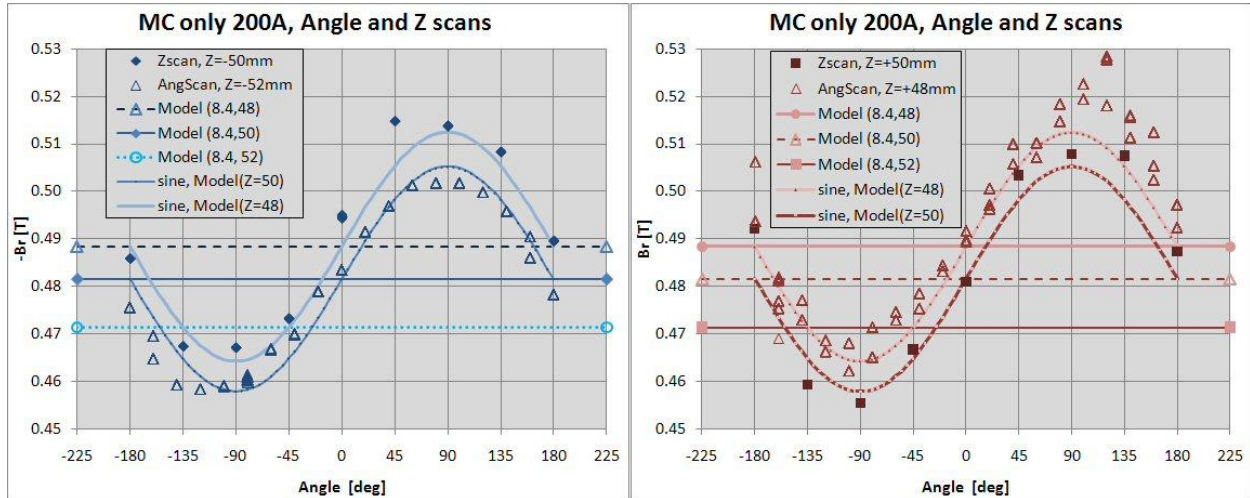


Fig. 29. Angle dependence of data for MC Angle Scans at $Z=175=-52$ mm ($-B_r$ left) and $Z=175=+48$ mm (B_r right), and Z scan data at ± 50 mm. Average B_r are shown for the as-built model at the same and nearby Z positions. Sinusoidal functions using the model parameters (and no angle offset) are plotted for some of the Z positions for comparison.

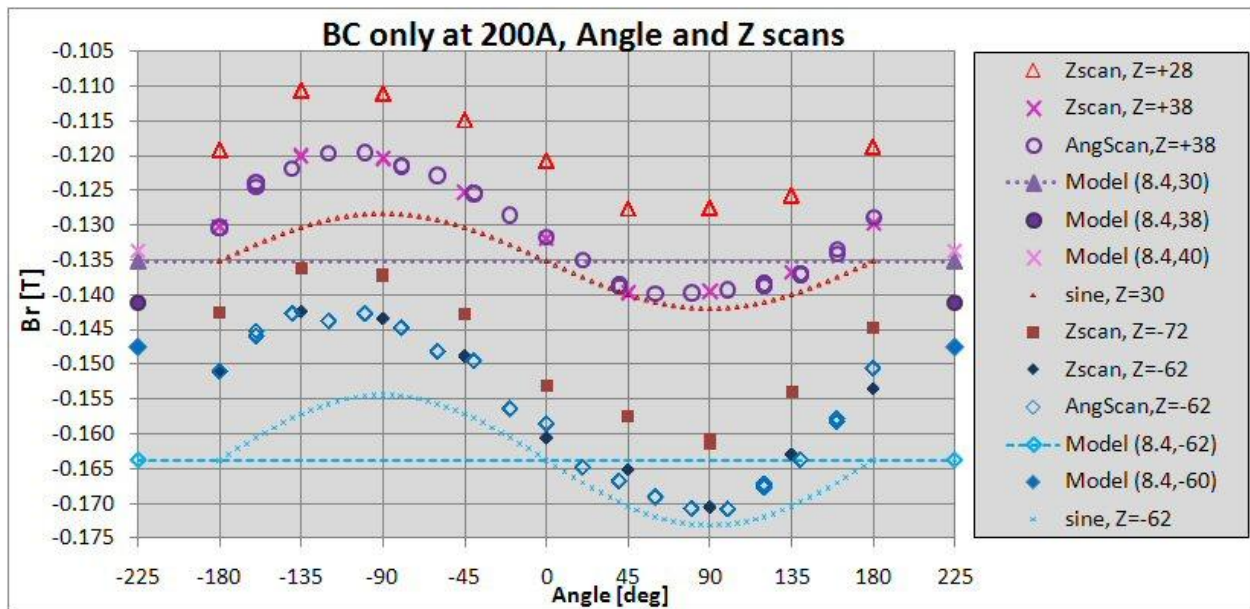


Fig. 30. Angle dependence of B_r data for BC Angle Scans at $Z=175 \sim +30$ and -72 mm, and Z scan data at ± 50 mm. Average B_r are shown for the as-built model at the same and nearby Z positions. Sinusoidal functions using the model parameters (and no angle offset) are plotted for some of the Z positions for comparison.

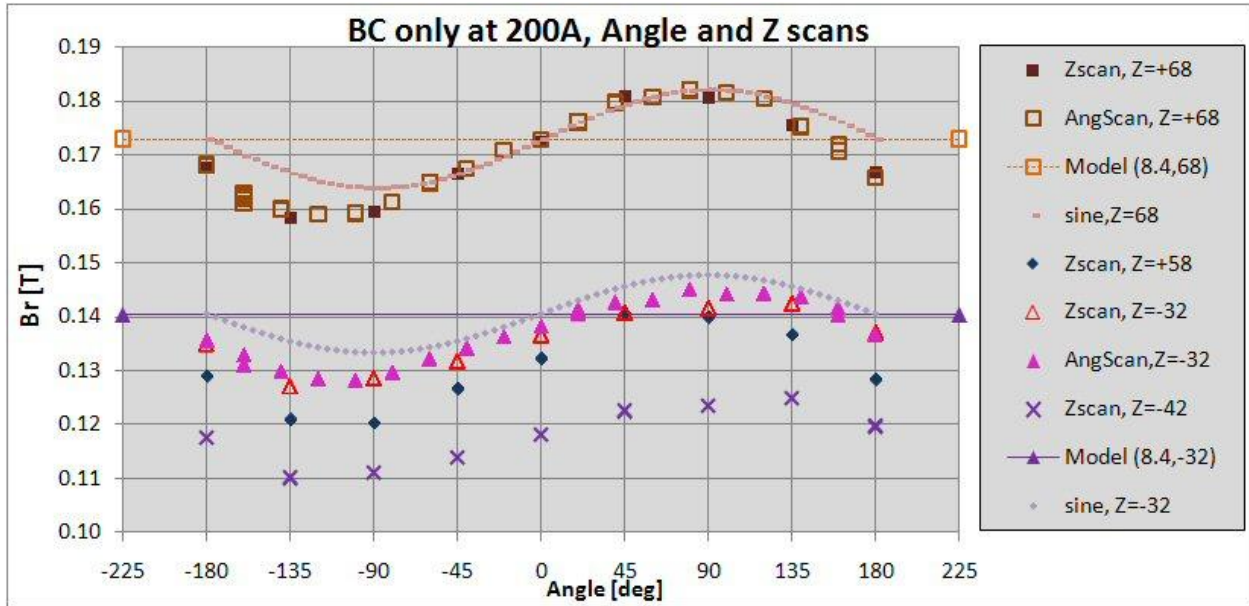


Fig. 31. Angle dependence of B_r data for BC Angle Scans at Z -175 ~ +70 and -30 mm, and Z scan data at ± 50 mm. Average B_r are shown for the as-built model at the same and nearby Z positions. Sinusoidal functions using the model parameters (and no angle offset) are plotted for some of the Z positions for comparison.

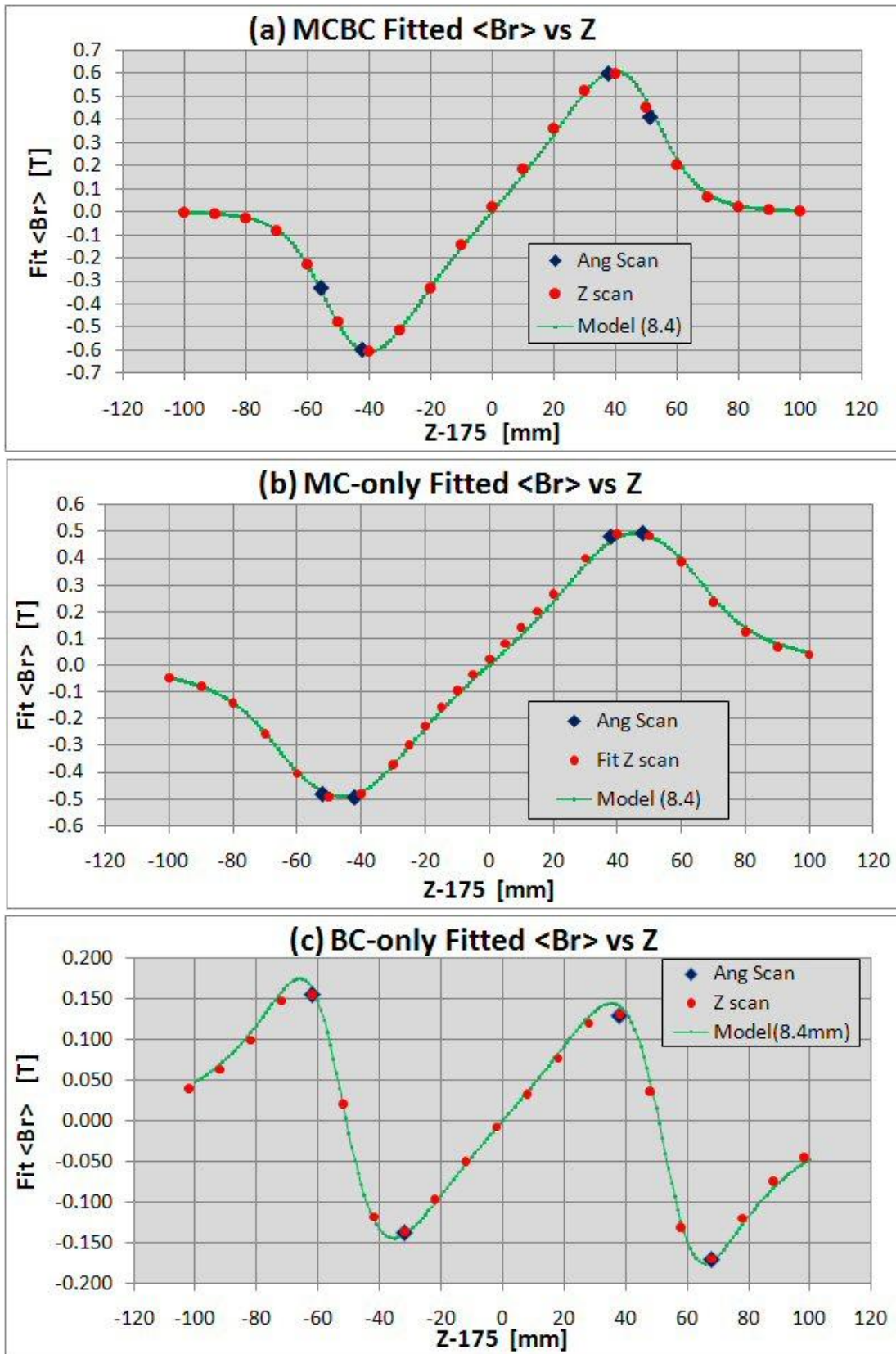


Fig. 32. Average B_r versus Z position, results from sinusoidal fits to angle dependence of B_r .

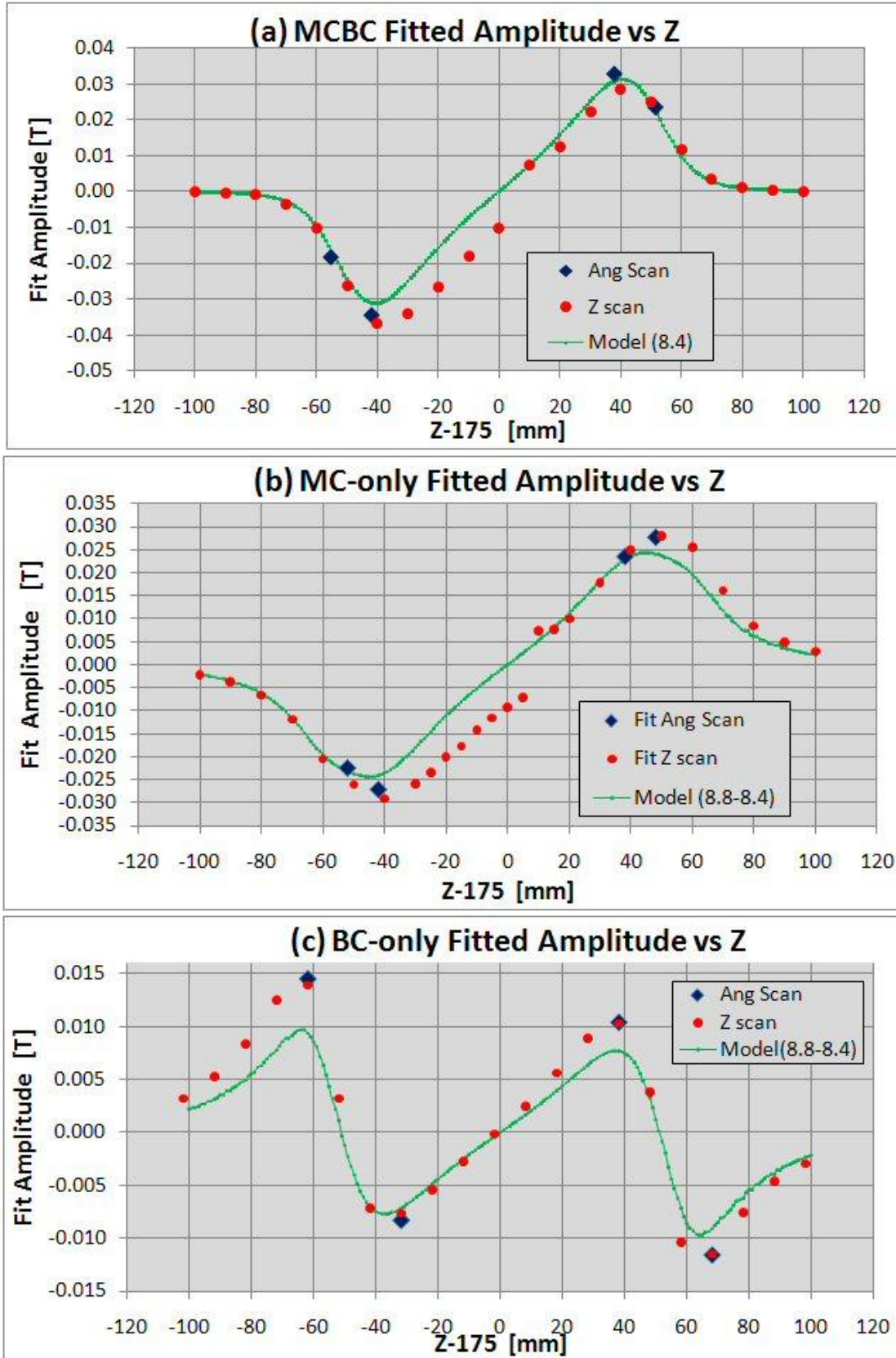


Fig. 33. Amplitude versus Z position, results from sinusoidal fits to angle dependence of B_r .

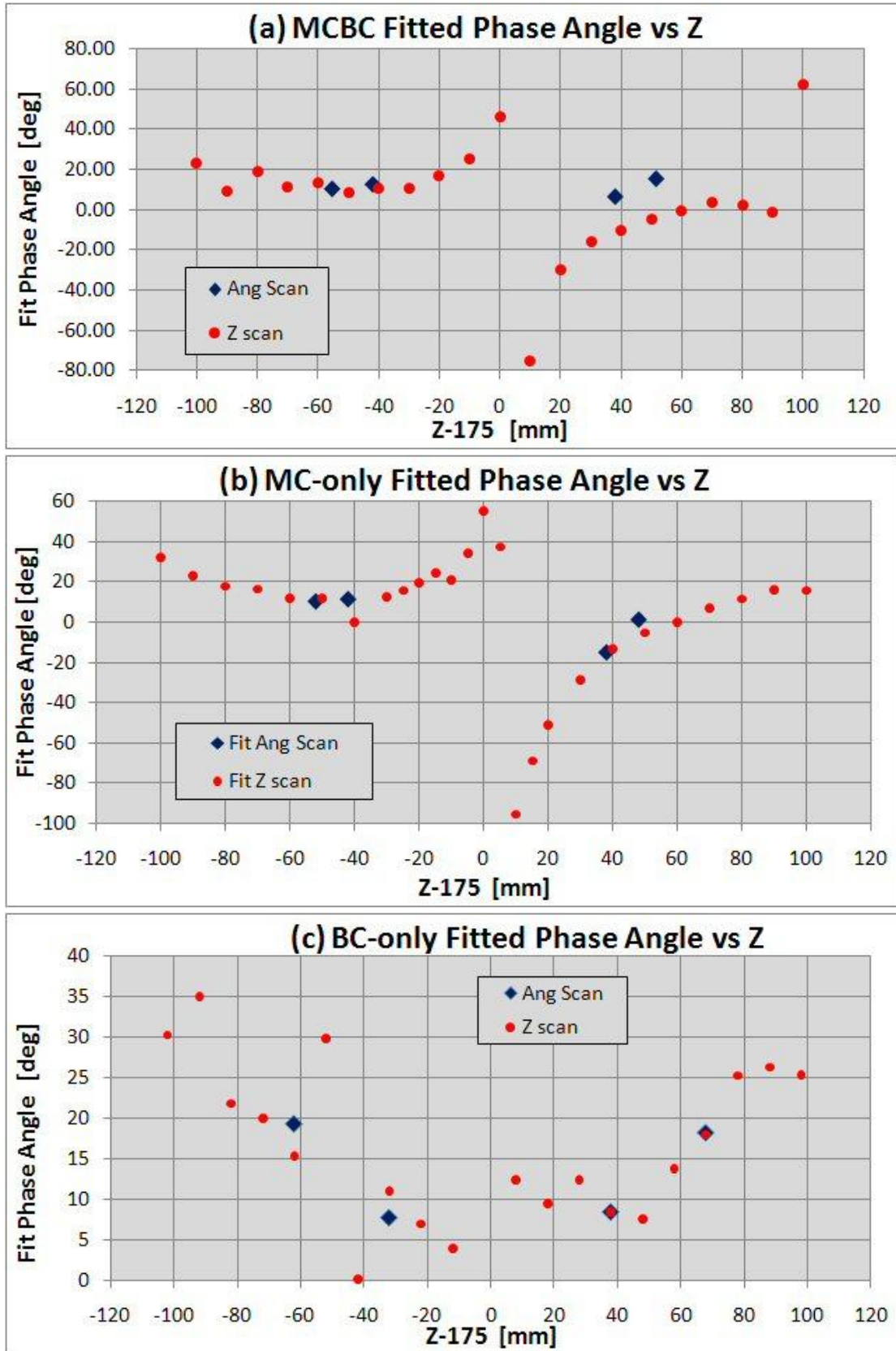


Fig. 34. Phase angle versus Z position, results from sinusoidal fits to angle dependence of B_r .

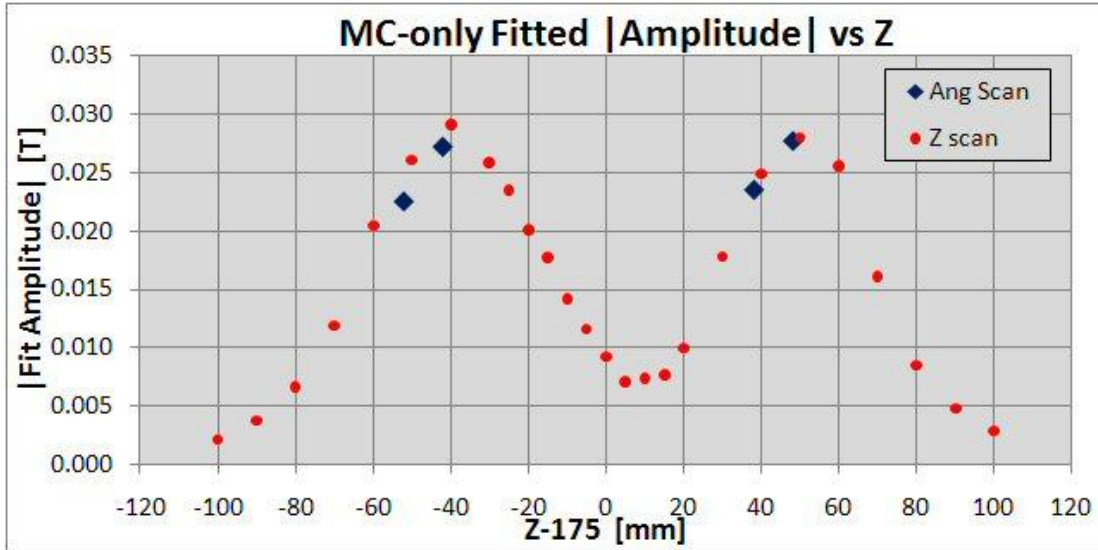


Fig. 35. Absolute value of fit amplitude versus Z position for MC angle.

VII. Conclusions

It is clear that the probe radius needed to explain the data is much larger than expected, 8.4 mm versus 7.6 mm, and this not physically possible (unless there is significant shrinkage of the probe parts, which is also not physically tenable: the maximum possible radius is achieved if the bearings ride along the warm bore inner wall, which gives a radius of 8.0 mm. Another possibility is that the manufacturer's dimension is incorrectly specified for the Hall probe element position with respect to the reference surface; this seems unlikely. Two possible explanations are that this discrepancy is either due to a problem with the model predictions, or that there is some distortion in the solenoid from perfect cylindrical symmetry that may cause distortions in the field. There is some evidence in the data to support this latter hypothesis, especially from fits to the angle dependence. A 3D model would be useful to explore this possibility quantitatively.

In general, this technique appears to work very well, as both Angle and Z scans give very consistent results. The apparatus for this first test resulted in somewhat larger errors in positioning the probe than were desired; nevertheless, the results suggest that it is indeed possible to determine the solenoid axis center at various positions along the length of the device, with a (not too well determined) precision on the order of 0.1 mm.

Further studies of this technique are planned, initially using the first production cryostatted CH solenoid assembly HCHB01. This will be done in a horizontal orientation using the same Hall probe apparatus, but with several improvements: first, the probe support bearings have been made with a closer tolerance fit onto the probe holder, and with an outer diameter that fits closely into the cryostat warm bore inner tube diameter (thus, the solenoid center will be mapped with respect to the warm bore tube axis). Second, the probe shaft itself will be shorter; third, a 3-axis Hall probe will be used in order to record B_r , B_z , and B_θ simultaneously at each Z position.

However, in this assembled cryostat, it is only possible to power the MC+BC configuration, as the coils are internally spliced together.

References

- 1] J. DiMarco, et al., "Certification of Superconducting Solenoid-Based Focusing Lenses," Submitted to Applied Superconductivity Conference ASC10, Fermilab-Conf-10-267-TD, August 2010.
- 2] J. DiMarco, M. Tartaglia, I. Terechkine, "Optical Properties of a CH-type Focusing Lens," TD-10-004, FNAL March 09, 2010
- 3] M. Tartaglia, et al., "Summary of HINS Focusing Solenoid Production and Tests," *IEEE Trans. Appl. Supercon.*, Vol. 20, No. 3, June 2010, pp.312-315.
- 4] M. A. Tartaglia, D. F. Orris, I. Terechkine, J. C. Tompkins, "Test Results for HINS Focusing Solenoids at Fermilab," *IEEE Trans. Appl. Supercon.* V19, no. 3, 1352-1355, June 2009.
- 5] B. Berkes, "Hall Generators," CERN Accelerator School on Magnetic Measurement and Alignment, CERN-92-05, pp. 167-192, March 1992.